國 立 交 通 大 學

光 電 工 程 研 究 所

碩士論文

氮化銦鎵/氮化鎵多重量子井發光二極體之特性與內部量子效率研究

Study on internal quantum efficiency and characteristic of InGaN/GaN multiple quantum well light emitting diode

研究生：柯智淳

指導教授：郭浩中 教授

盧廷昌 教授

中 華 民 國 九 十 八 年 六 月

氮化銦鎵/氮化鎵多重量子井發光二極體之電特性與內部量子效率研究

Study on internal quantum efficiency and characteristic of InGaN/GaN
multiple quantum well light emitting diode

研究生：柯智淳   Student: Chih-Chun Ke
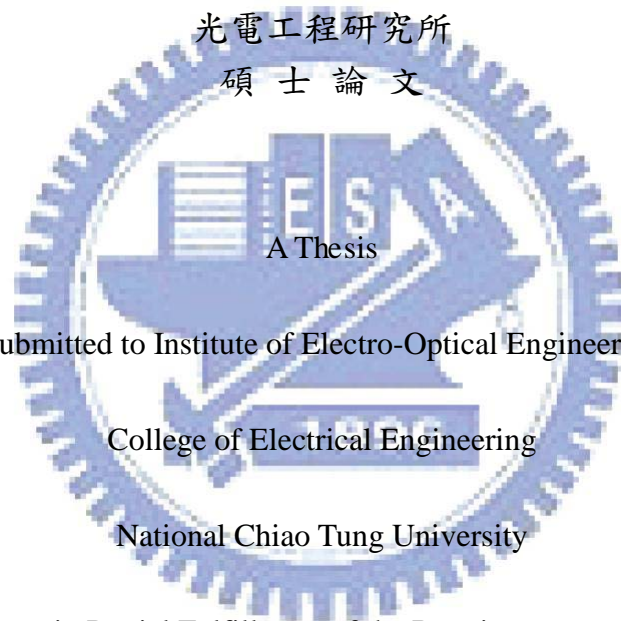
指導教授：郭浩中 教授   Advisor: Prof. Hao-Chung Kuo

盧廷昌 教授   Prof. Tien-Chang Lu

國 立 交 通 大 學

光 電 工 程 研 究 所

碩 士 論 文

A Thesis

Submitted to Institute of Electro-Optical Engineering

College of Electrical Engineering

National Chiao Tung University

in Partial Fulfillment of the Requirements

for the Degree of

Master

In

Electro-Optical Engineering

June 2008

Hsinchu, Taiwan, Republic of China

氮化銦鎵/氮化鎵多重量子井發光二極體之特性與內部量子效率研究

研究生：柯智淳　　　　　　　　　　　　　指導教授: 郭浩中教授

　　　　　　　　　　　　　　　　　　　　　　　盧廷昌教授

國立交通大學光電工程研究所碩士班

摘要

　　本論文中，我們利用有機金屬氣相沉積法成長在不同的藍寶石基板上，前者為成長在圖案化藍寶石基板(Patterned sapphire substrate, PSS)之氮化銦鎵/氮化鎵(InGaN/GaN)多重量子井(Multiple quantum well, MQW)，後者為成長在一般藍寶石基板。我們利用光激發螢光(Photoluminescence, PL)、電激發螢光(Electroluminescence, EL)、以及Advanced Physical Models of Semiconductor Devices (APSYS)模擬軟體等進行樣品的光學與電特性分析。

　　我們藉由變功率光激發螢光和低溫電激發螢光量測去探討低溫和室溫時，影響氮化銦鎵/氮化鎵多重量子井發光二極體內部量子效率(Internal quantum efficiency, IQE)之物理機制，發現氮化銦鎵/氮化鎵多重量子井發光二極體之內部量子效率會隨著雷射激發功率而變化，主是受到量子井內之非輻射複合中心以及量子井內之量子侷限史塔克效應(Quantum confined Stark effect, QCSE)與能帶填滿效應(Band filling effect)所影響。在本研究中，也利用了理論模型去計算內部量子效率，計算得到的內部量子效率與實驗結果幾乎吻合。

　　另外由低溫電激發螢光量測，我們發現當在低溫高電流注入時，電洞會因為溫度變化造成的載子濃度以及遷移率下降，造成電洞在量子井中的分布不均勻，且因為電洞的遷移率下降，造成更多的電洞無法有效的注入到量子井中而累積在靠近p-GaN的量子井中，另外也由於量子井中電洞的不足，造成更多的電子會產生溢流現象，導致內部量子效率在高電流下會產生效率遽降的情況。

Study on electrical characteristic and internal quantum efficiency of InGaN/GaN multiple quantum well light emitting diode

Student : Chih-Chun Ke

Advisor: Prof. Hao-Chung Kuo

Prof. Tien-Chang Lu

Institute of Electro-Optical Engineering

National Chiao Tung University

Abstract

In this study, we studied two kinds of structures grown by metalorganic chemical vapor deposition (MOCVD). The samples of InGaN/ GaN MQW ultraviolet light emitting diode (UV LED) were grown on c-plane patterned and conventional sapphire substrate. The photoluminescence (PL), low temperature electroluminescence system (LTEL) and Advanced Physical Models of Semiconductor Devices (APSYS) were performed to investigate the optical and electrical properties of the grown samples.

This research intends to investigate the physical mechanisms of excitation power and injection current dependent internal quantum efficiency (IQE) in InGaN/GaN MQW LEDs at 15 K and 300 K for PL and 30 K and 300 K for EL. The dependence of the IQE on excitation power density has been observed, we confirmed the variation of IQE with increasing excitation power is due to the coulomb screening of quantum confined Stark effect (QCSE) and band-filling effect in InGaN/GaN QW. Moreover, the nonradiative recombination has to be taken into account at lower excitation power. We also used the theoretical model to calculate the IQE; the calculation of IQE

coincides with our experimental results.

From the low temperature electroluminescence measurement, the hole concentration distribution is not uniform which can be attributed to the hole mobility decreased at low temperature resulting in hole couldn't transport to the later QW effectively. Under this condition where thermal generation of holes is insufficient and injected electrons continuously deplete holes, some of the injected electrons reach the *p*-GaN and exit the system without being able. Consequently, the results verified the EL efficiency droop more rapidly at lower temperature.
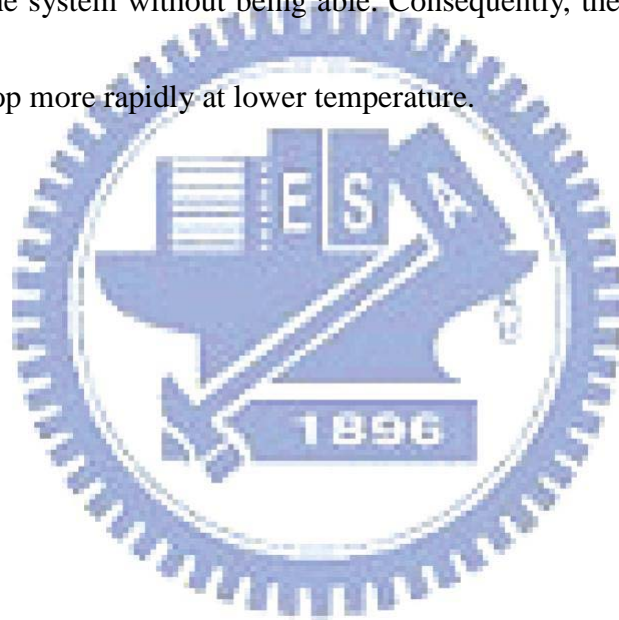
誌謝

在打這篇誌謝文的同時，真的有要畢業的感覺。每次在暗房裡跟儀器奮戰到深夜，每次報告前緊張的反覆演練，現在想起來，好像是昨天才發生的事情。在這裡，我要感謝在我碩士兩年生活中的許多人，在我遇到困難時對我伸出援手，

在我遇到問題時不吝幫我解答，使我可以順利的完成我的碩士學位。

首先，我由衷的感謝王興宗老師的指導，老師做學問認真的態度深深地影響我，而在每次報告時老師的殷切叮嚀，我都有牢記在腦海裡；感謝郭浩中老師在我實驗上遭遇困難時，給予我幫助，以及感謝老師平時對我的鼓勵，使我遇到挫折時能更勇敢的面對；感謝盧廷昌老師的指導，使我能夠有許多想法去解決實驗上所遇到的問題。

感謝清華學長，平常Meeting上的指導以及對研究上的規劃和叮嚀，每當我開始怠惰，總是有學長在旁邊鞭策，以及研究上給予的幫助；感謝明華學長，我總追著你問很多光學儀器與光學實驗的問題，每次你都不厭其煩的幫助我，也不時會對於實驗上提供不少想法，因為你和清華學長的協助，我才能更順利的完成我的實驗。感謝明權學長和瑋婷學妹，最後的低溫EL實驗，若沒有你們的幫忙，我自己一個人應該會更辛苦，和你們一起做實驗真的蠻快樂的，由衷的謝謝你們。感謝政暐同學，從大學專題到碩士，在實驗上的問題總是會和你一起討論，也常常會跟你抱怨實驗的不順利，謝謝你平常對我的鼓勵；感謝小馬、阿綱、治凱、勁生、玟君、睿中、啄木、尚樺等碩二的同學，因為你們而讓我的碩士生活更多采多姿。感謝小昕和依嚀學弟妹，常常陪著我做實驗到很晚；感謝永吉學弟，總是去麻煩你模擬上的問題，對於模擬的理論也從你那學到很多

感謝所有的學長學弟妹們，每當我做實驗沒空吃飯時，總是會有人幫忙買飯和飲料，每當實驗做到很辛苦時，總是有人相伴聊天，實驗室的笑聲總是會讓我感到很開心，跟著大家一起吃飯聊天總讓我會忘掉實驗上的辛苦。

最後謝謝我的家人，感謝我的爸爸媽媽支持，讓我順利完成學業，謝謝你們。

Content

Chapter 1 Introduction

Chapter 2 Properties of Ⅲ-Nitride semiconductor

Chapter 3 Experimental instrument and setup

Chapter 4 Excitation power dependent and theoretical model of calculation IQE in InGaN/GaN multiple quantum wells grown on patterned sapphire substrate

Chapter 5 Analysis of electroluminescence and efficiency droop in InGaN/GaN multiple quantum wells grown on patterned sapphire substrate

List of Tables

List of Figures

Chapter 1 Introduction

1.1 Development of Nitride-Based Light-Emitting Diodes

In recent decades, the III-nitrides InN, GaN, and AlN related alloys become an interesting class of wide bandgap materials and play an important role in semiconductor devices [1-7], especially for optoelectronics [1-3] as well as electronics. Since the wurtzite polytypes of III-nitrides form a continuous alloy system whose direct bandgap ranging from 0.7 eV for InN [8], to 3.4 eV for GaN, and to 6.2 eV for AlN [9], the optical devices using III-nitrides could be activated at wavelength ranging from red, green, blue, to deep ultraviolet. This phenomenon is quite different from other III-V materials systems based on GaAs, AlAs, InAs, GaP and related alloys. In addition, the III-nitrides materials are expected to be superior to the counterparts made of Si and other III-V materials for high-temperature and high-power applications [4-7].

The first blue light-emitting diode (LED) using III-nitrides materials was fabricated by J. I. Pankove *et al.*[10] with an metal-i-n structure in 1972. Since that, related research is going on continually. However, progresses have been limited because of highly background *n*-type concentration resulting from the native defects commonly thought to be nitrogen vacancies and residual impurities such as Si and oxygen acted as an efficient donor, poorly conducting *p*-type GaN, and the lack of

appropriate substrates for epitaxial growth. Until late 1980s, H. Amano *et al.* [11, 12]

discovered a very useful application of a low-temperature buffer layer and developed

low-energy electron beam interaction (LEEBI) techniques to obtain better GaN

epilayer and conductive *p*-type GaN, initiated a new strong interest in this research

field. Finally, the first GaN-based blue LED constructed of a real p-n junction was

achieved, which had greatly improved in the device performance. However, the

acceptor concentration of *p*-type GaN is still too low such that the application of these

materials is still unreliable. After that, S. Nakamura *et al.* [13] achieved better

conductive *p*-type GaN material by introducing a simple thermal annealing procedure

in nitrogen ambient ($\geqq$ 750 ℃). The thermal annealing process represent that an

easy, reliable, and conventional method for obtaining a high conductively *p*-type GaN.

With these technique developments and achievements, the full-color semiconductor

lighting age has become a reality.
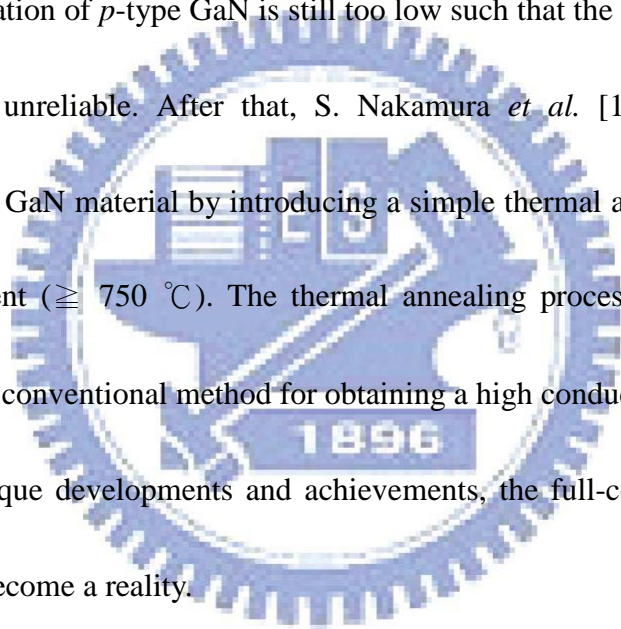
1.2 Characteristic of Nitride-Based Ultraviolet Light Emitting Diodes

GaN-based ultraviolet light emitting diodes (UV LED) tend to be less efficient as

the emission wavelength decreases. It is well known that high efficiency radiative

recombination in dislocated blue and green InGaN multiple quantum wells LEDs has

been attributed mainly to the localized states due to indium phase separation or

fluctuation in the $In_xGa_{1-x}N$/GaN quantum wells [14-17]. For UV LEDs, the InN mole

fraction in the InGaN well is lower than that of the blue or green ones. Since phase

separation may does not occur at low In composition [18], it is proposed that less

localized states leads to lower external quantum efficiency of UV LED. T. Mukai and

S. Nakamura performed a comparative study on GaN and InGaN UV (360-380nm)

LEDs grown on sapphire substrate and epitaxially laterally regrown GaN substrates

(ELOG), respectively [19].

Based on the quantum confinement investigation of the GaN-based LEDs,

localized state formed by composition fluctuation in the quantum wells was still

considered a key factor for high quantum efficiency. The effect of dislocation density

on the external quantum efficiency of UV LEDs supports the postulate as well. On the

other hand, carrier overflow, particular in the conduction band, can also be the origin

of low quantum efficiency from a theoretical point of view because the potential well

of an UV LED is much lower than that of its blue and green counterparts. It has also

been reported that band-to-band instead of localized state emission is the dominant

emission mechanism in AlInGaN/InGaN UV (~ 420nm) LEDs [20]. Therefore,

dislocation density and carrier confinement have become very important to improve

the light performance of UV LEDs.

Shown in Fig. 1.1 is the benchmark of history development of UV LED in the

wavelength range from 370 to 410 nm. From the benchmark, it can be deliberated that

the UV LED has a vigorous development after 1999. It is worthy to note that the near

UV LED had a great improvement by using lateral epitaxy on patterned substrate

(LEPS) in 2001 [21]. The enhancement of output power is attributed to the reduction

of dislocation density and light extraction by the patterned substrates. It is well known

that the nitride-based visible optoelectronic devices, grown along the polar [0001]

c-direction, are characterized by the presence of polarization induced electric fields in

the multiple quantum wells (MQWs). These electric fields, caused by both

discontinuities in spontaneous and piezoelectric polarization at heterointerfaces, lead

to the quantum confined Stark effect (QCSE), which would cause charge separation

between holes and electrons in quantum wells and lower radiative recombination

probability [22, 23]. This is one of the primary reasons why thin quantum wells are

employed in c-plane LEDs. Additionally, the peak emission wavelength of LEDs

grown on c-plane GaN would cause blue-shifted with increasing drive current due to

screening of the internal fields.

Conventional GaN-based LEDs are grown on top of sapphire substrates with a

low temperature GaN or AlN nuclear layer. Although the introduction of low

temperature GaN or AlN nuclear layer could significantly improve the crystal quality

of the subsequent GaN epitaxial layer, threading dislocation density in the order of

$10^9 \sim 10^{12}$ cm^2 will still remain in the sample due to the large difference in lattice constant and thermal expansion coefficient between sapphire and GaN. Previously, it has been shown that one can effectively reduce the threading dislocation density down to 10^7cm^2 or less by using the so-called epitaxial lateral over growth of GaN (ELOG). In order to achieve such an ELOG, one need to grow a 2~3 μm-thick GaN epitaxial layer on sapphire substrate first, pattern the sample, and then perform the second MOCVD growth. In other words, we need to perform the MOCVD growth twice.

Recently, it has been reported that one can also reduce the threading dislocation density in GaN by growing GaN epitaxial layers on top of patterned sapphire substrates. By using the patterned sapphire substrates, Tadatomo *et al.* [24] have successfully fabricated high output power nitride-based UV LEDs with large external quantum efficiency. To this end, there are several ways to increase the light extraction efficiency, including shaping of LED dies [25], flip-chip mounting [26], roughening of the top LED surface [27],[28], growth on a patterned sapphire substrate [29],[30], and the use of reflectors [31],[32]. Yet, in each of the above cases, the light extraction efficiency of UV LEDs becomes lower than that of visible LEDs due to a severe light absorption by transparent electrodes, bonding pads, and wire bonds in the package.

1.3 Motivation

Typical InGaN/GaN LED are characterized by a substantial decrease in

efficiency as injection current increases. This phenomenon which known as efficiency

droop is a severe limitation for high power devices that operate at high current

densities and must be overcome to enable the LEDs needed for solid-state general

illumination. The efficiency droop is caused by a nonradiative carrier loss mechanism,

which is small at low currents but becomes significant for high injection currents.

Competition between radiative recombination and this droop-causing mechanism

results in the reduction in efficiency as current increases. The physical origin of

efficiency droop remains controversial, and several different mechanisms have been

suggested as explanations, including carrier leakage from the active region

[33][34][35]. Auger recombination [36], junction heating [37], and carrier

delocalization from In-rich low-defect-density regions at high carrier densities

[38],[39]. Carrier leakage in GaInN LEDs generally refers to the escape of electrons

from the active region to the p-type region. These leakage electrons may then

recombine with holes either in the p-type region or at the contacts, dominantly by

nonradiative processes. Necessarily, therefore, fewer holes than electrons are injected

into the active region. These two phenomena that escape of electrons form the active

region and reduced hole concentration of any carrier leakage explanation for droop.

Hole injected into the active region may be the limiting factor, possibly due to the low

p-type doping efficiency or the electron blocking layer (EBL) acting as a potential

barrier also for holes. As a result of the low hole injection, current across the device is dominated by electrons. Devices with p-type active regions which should increase hole injection efficiency have been proposed as a solution to this problem.

However, it is not clear which cause the efficiency droops at high current. For this study, we discussed the temperature dependence IQE as a function of injection current density clearly. By investigating the excitation power dependence PL intensity at low and room temperature, we can obtained the value of IQE, Then, we study the temperature dependence EL intensity as a function of injected current density and APSYS simulation, the physical mechanisms of current dependent IQE of InGaN/GaN UV LED has been confirmed.

This thesis is organized in the following way: In chapter 2, we give some theoretical backgrounds and characteristics about InGaN/GaN MQW structures. The experimental setups and theory are stated in chapter 3. In chapter 4, we present the experiment results and discuss for optical properties of InGaN/GaN MQW UV LED grown on conventional and patterned sapphire substrates. In chapter 5, we show the experiment results and discuss for physical mechanisms of temperature dependence IQE as a function of injection current density in InGaN/GaN UV LEDs. Finally, we gave a brief summary of the study in chapter 6.
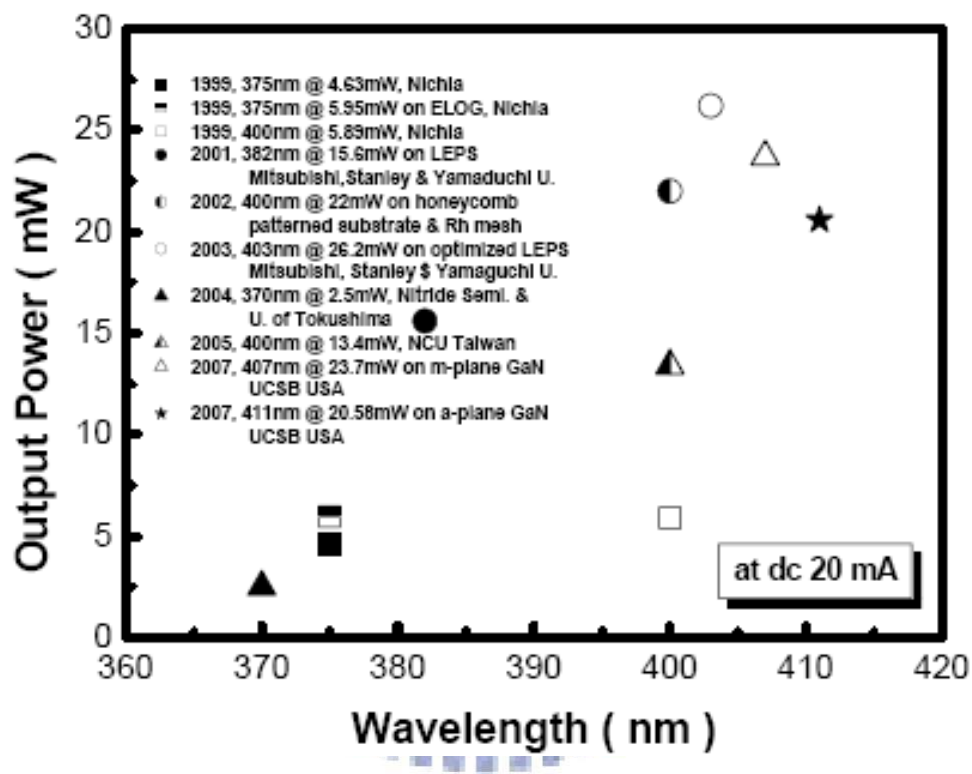
Fig. 1.1 Benchmark of UV LED in the wavelength range from 370 to 410 nm.

Chapter 2 Properties of Ⅲ-Nitride semiconductor

In this chapter, we show the definition of internal quantum efficiency (IQE), light extraction efficiency (LEE), and external quantum efficiency (EQE). Finally, we show the properties and advantages of InGaN/GaN MQW grown on patterned sapphire substate (PSS).

2.1 Internal quantum efficiency (IQE)

The active region of ideal LED emits one photon when one electron injected. Each charge quantum-particle (electron) produces one light quantum-particle (photon). Thus the ideal active region of an LED has a quantum efficiency of unity. The internal quantum efficiency is defined as:

$$\eta_{int} = \frac{number\ of\ photons\ emitted\ from\ active\ region\ per\ second}{number\ of\ electrons\ injected\ into\ LED\ per\ second} = \frac{P_{int}/h\nu}{I/e}$$

where P_{int} is the optical power emitted from the active region and I is the injection current. Photons emitted by the active region should escape from the LED die. In an ideal LED, all photons emitted by the active region are also emitted into free space. Such an LED has unity extraction efficiency. However, in a real LED, not all the power emitted from the active region is emitted into free space. Some photons may never emit into the free space. This is due to several possible loss mechanisms. For example, light may be reabsorbed by material itself of the LED. Light may be incident

on a metallic contact surface and be absorbed by the metal. In addition, the phenomenon of the total internal reflection, also refereed to as the trapped light phenomenon, reduces the ability of light to escape from the active region.

Another view point, the internal quantum efficiency in a semiconductor is related to non-radiative recombination centers. If the radiative lifetime is denoted as τ_r and the non-radiative lifetime is denoted as τ_{nr}, then the total probability of recombination is given by the sum of the radiative and non-radiative probability:

$$\frac{1}{\tau} = \frac{1}{\tau_r} + \frac{1}{\tau_{nr}}$$

(2.1.1)

The relative probability of radiative recombination is given by the radiative probability over the total probability of recombination. Thus the probability of radiative recombination or IQE is given by:

$$\eta_{int} = \frac{\tau_r^{-1}}{\tau_r^{-1} + \tau_{nr}^{-1}}$$

(2.1.2)

The IQE gives the ratio of the number of light quanta emitted inside the semiconductor to the number of charge quanta undergoing recombination. Note that not all photons emitted internally may escape from the semiconductor due to critical angle and reabsorption mechanisms.

By the above equation, the internal quantum efficiency is determined by the competition between radiative and nonradiative recombination processes. In this material system, the radiative recombination rate is affected by the quantum-confined Stark effect (QCSE) and exciton localization effects. Although the relative importance of these contributions has been widely studied in recent years, many questions regarding the emission process still remain.

2.2 Light extraction efficiency (LEE) and external quantum efficiency (EQE)

The extraction efficiency can be a severe limitation for high performance LEDs. It is quite difficult to increase the extraction efficiency beyond 50% without resorting to high sophisticated and costly device processes. The light extraction efficiency (LEE) is defined as:

$$\eta_{\text{extraction}} = \frac{\text{number of photons emitted into free space per second}}{\text{number of photons emitted from active region per second}} = \frac{P/h\nu}{P_{\text{int}}/h\nu} \quad (2.2.2)$$

where P is the optical power emitted into free space. Considering the refractive indices of GaN (n = 2.5) and air, for the light escape cone is about 23% due to the critical angle. Assuming that light emitted from sidewalls and backside is neglected, one expects that approximately only 4% of the internal light can be extracted from a

surface. The light outside the escape cone is reflected into the substrate and is repeatedly reflected, then reabsorbed by active layers or electrodes, unless it escapes through the sidewalls. However, there is much room for improvement of the light extraction efficiency. For example, roughening of the top LED surface increased the light extraction efficiency.

Finally, the external quantum efficiency (EQE) is defined as:

$$\eta_{ext} = \frac{number\ of\ photons\ emitted\ into\ free\ space\ per\ second}{number\ of\ electron\ injected\ into\ LED\ per\ second} = \frac{P/h\nu}{I/e} = \eta_{int}\eta_{extraction} \quad (2.2.3)$$

from the above equation, we can know that the EQE depend on IQE and LEE, therefore, the improvement of IQE and LEE pay an important role of LED. Recently, the patterned sapphire substrate is introduced to improve the IQE which is attributed to reduce the dislocation density and enhance the LEE due light emit to substrate may reflect and emit into free space.

2.3 Properties of LED grown on patterned sapphire substrate

However, owing to the large mismatch (~14%) of lattice constant [40] and thermal expansion (~25%) between epitaxial GaN films and sapphire substrates,[41] high density dislocations ranging from $10^8 \sim 10^{10}$ cm^{-2} degrade the light-emitting diode (LED) performance profoundly. Thus, growth of GaN with low-density dislocations

has been a major effort for fabrication of reliable high-efficiency LEDs. By epitaxial

lateral overgrowth (ELOG) with SiN_x or SiO_2 mask patterned on as-grown GaN seed

crystal, threading dislocations can be significantly eliminated. Although this

overgrowth technique can dramatically improve crystalline quality, the requirement of

two-step growth procedure is time-consuming and easily introduced contaminations.

In recent years, the single growth technique by introducing patterned sapphire

substrates (PSS) has been extensively researched. The simplified growth method can

reduce the threading dislocations and increase the light extraction. The geometrical

shape of the sapphire patterns can effectively scatter or redirect the guided light inside

an LED chip to find escape cones, such as the hemispherical shape made by the dry

etching technique [42] and the inclined *c*-plane facet of sapphire made by the wet

etching technique [43]. In brief, the patterned sapphire substrate has some benefits:
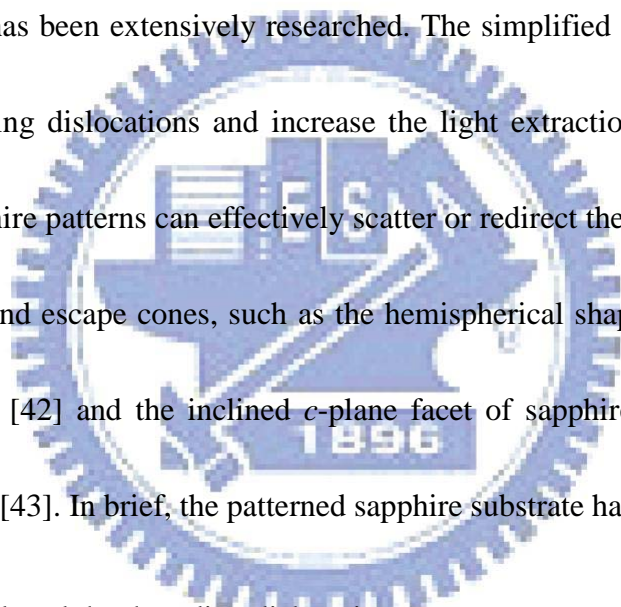
(1) Reduced the threading dislocation

(2) Single growth process without any interruption

(3) Increases the emitting light extraction efficiency

Fig. 2.3.2 displays the schematic illustration of increased light extraction

efficiency. Another technique is chemical wet etching which is a promising technique

for preparing PSS show in Fig. 2.3.1, without the need for expensive inductively

coupled plasma (ICP) used in dry etching. The characteristic inclined crystallographic facets resulting from wet etching can facilitate superior light extraction efficiency. Wet-etching causes less damage to the substrate than dry etching does, hence the sapphire surface damage induced by dry etching can be eliminated. In this study, we prepared two samples grown on conventional and patterned sapphire substrates. Cross sectional of SEM micrographs of the patterned sapphire substrate is shown in Fig. 2.2.3. The lens height and diameter of the patterned sapphire are 1.4 and 3.5 μm, respectively. The distance between each lens is 1.0 μm. We can observe the lens pattern is uniformly arranged and homogeneous size distribution. In the normal wedge shape pattern, one could reduce the threading dislocation whereas the optical emission is not enhanced appreciably. On the other hand, by using lens shaped PSS, TD density can be reduced and also optical emission efficiency could be improved due to internal reflection in the lens.
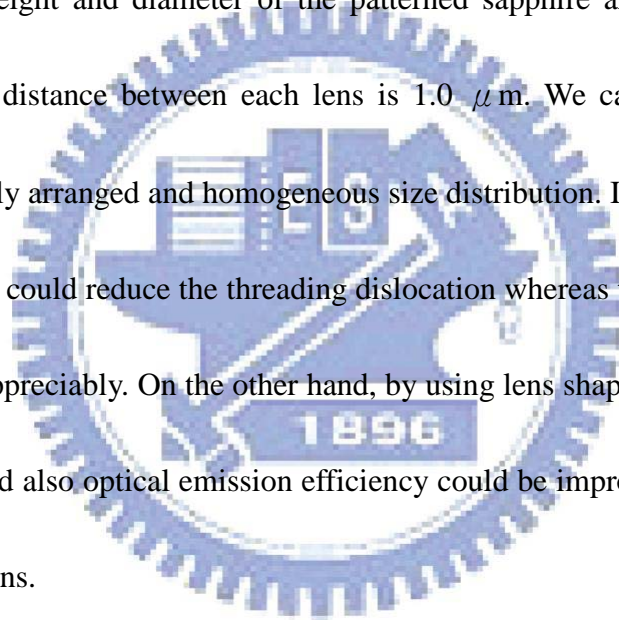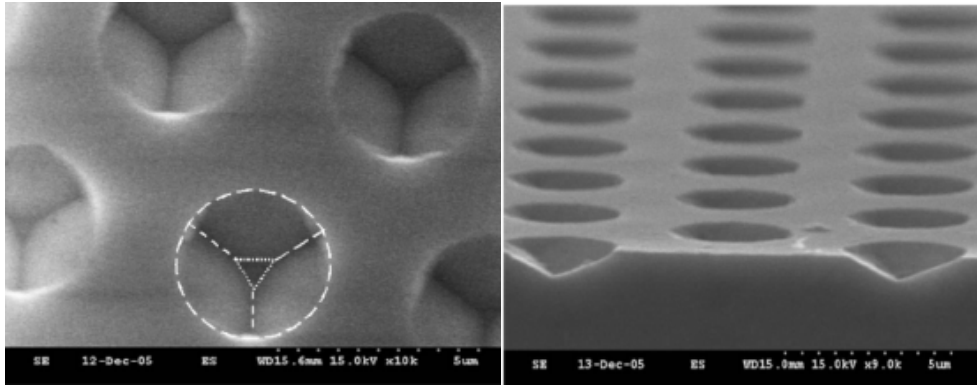
Fig. 2.3.1 Top and cross-sectional view SEM images of a PSS by wet etching
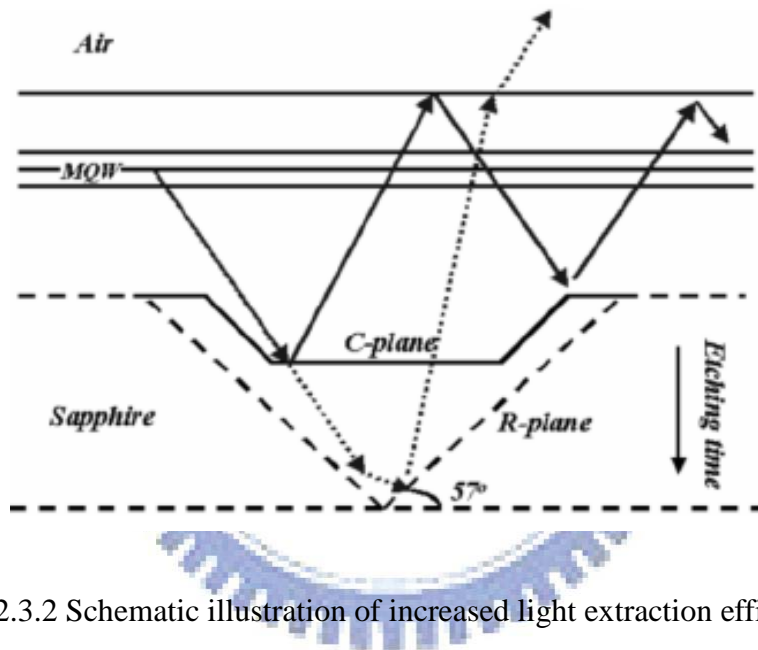
Fig. 2.3.2 Schematic illustration of increased light extraction efficiency
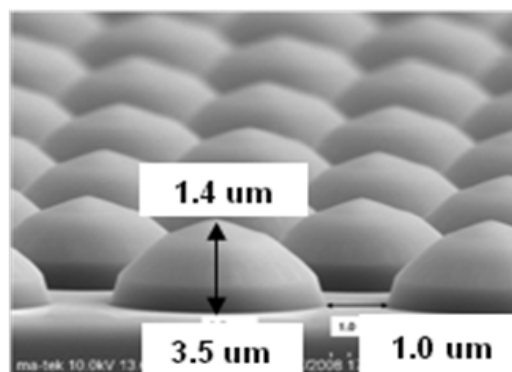
Fig. 2.3.3 SEM morphologies of PSS

Chapter 3 Experimental instrument and setup
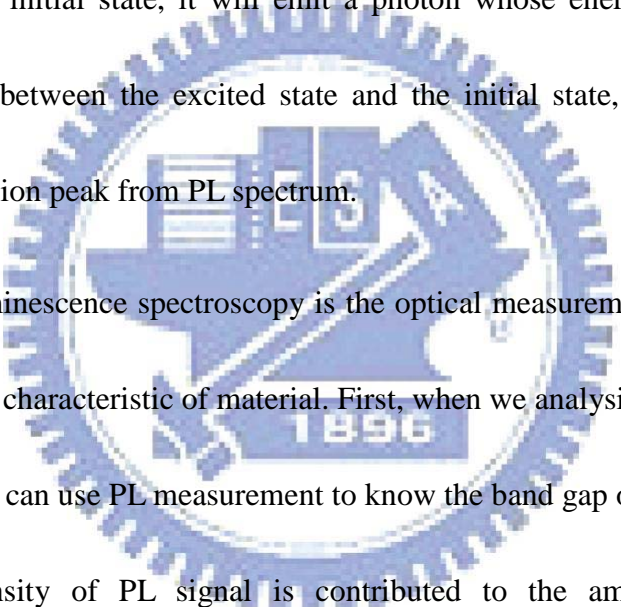
3.1 Sample structure and Fabrication

The sample in this study are commercial InGaN/GaN MQW UV LEDs and grown by metalorganic chemical vapor deposition (MOCVD). The sample in this study grown on c-plane (0001) sapphire substrates and patterned sapphire substrate (PSS), respectively. The sample structure consist $1.5\,\mu$m undoped n-GaN, a $2\,\mu$m Si-doped n-type GaN, and an unintentionally doped active layer with $In_xGa_{1-x}N$/GaN MQWs, and a 20nm p-AlGaN electron blocking layer (EBL), a 50nm p-$Al_{0.2}Ga_{0.95}N$, and 20nm Mg-doped p-type GaN. The doped concentration of n- and p-type GaN is nominally 5×10^{18} and 1×10^{19} cm^{-3}, respectively, the MQWs layer comprise 6 periods InGaN well (~2.5 nm) and GaN barrier (~1.5 nm). The sample structure is shown in Fig. 3.1.1. The fabrication processes of InGaN/GaN UV LED show in Fig. 3.1.2. In this study, we is interested in the reduction of dislocation density of InGaN/GaN UV LED on PSS which may affect the internal quantum efficiency and the efficiency droop at high current, hence, we will study the relation between defects and physical mechanisms of quantum efficiency.

3.2 Photoluminescence (PL)

PL spectroscopy has been used as a measurement method to detect the optical

properties of the materials because of its nondestructive characteristics. PL is the emission of light from a material under optical excitation. The laser light source used to excite carriers should have larger energy band gap than the semiconductors. When the laser light is absorbed within the semiconductors, it would excite the carriers from the valence band to the conduction band. Then, it produces the electrons in the conduction band and the holes in the valence band. When the electron in an excited state return to the initial state, it will emit a photon whose energy is equal to the energy difference between the excited state and the initial state, therefore, we can observed the emission peak from PL spectrum.

The photoluminescence spectroscopy is the optical measurement to examine the quality and optical characteristic of material. First, when we analysis a new compound semiconductor, we can use PL measurement to know the band gap of the new material. Second, the intensity of PL signal is contributed to the amount of radiative recombination in the materials. Therefore, PL measurement can be used to understand the material quality and the recombination mechanisms of the materials.

The carrier recombination processes occur in many ways in order to reach the equilibrium. Those processes can be divided into radiative recombination and nonradiative recombination. We can recognize the radiative recombination easily at low temperature by PL measurement, since it would not be influenced by the thermal

energy.

If there are some defect energy level existed in energy band gap of semiconductor, they also could contribute to radiative recombination process. Therefore, we could observe the multiple emission peaks in the PL spectrum, and the intensity of the emission peaks is related to the contribution of the individual radiative recombination process.

The schematic setup of our PL system is shown in Fig. 3.2.1. The pumping source was a multi-mode and non-polarized Helium-Cadmium laser operated on 325 nm with 35 mW. After reflecting by three mirrors, the laser light was focused by a lens which focal length was 5 cm, to 0.1 mm in diameter and the luminescence signal was collected by some lens. The probed light was dispersed by 0.32 monochromator (Jobin-Yvon Triax-320) with 1800, 1200, and 300 grooves/mm grating and the maximum width if the entrance slit was 1 mm. In order to prevent the laser coupling with the PL spectrum, we used the long pass filter in front of the entrance slit. In the temperature-dependent PL measurement, all the samples were placed in the closed-cycle cryostat with a temperature controller ranging from 20 K to 300 K.

3.3 Time-resolved photoluminescence (TRPL) and IQE measurement system

Time-resolved photoluminescence (TRPL) is an indispensable technique to study

the dynamical process of photoexcited carriers such as relaxation, radiative, nonradiative, and localization processes. The transient luminescence intensity obtained by the data of TRPL is generally expressed by the following equation as a function of time after excitation:

$$I(t) = I(0)\exp(-\frac{t}{\tau})$$

(3.3.1)

The pulsed excitation source for the IQE measurement is provided by the frequency doubler (2w) or frequency tripler (3w) beams of a mode-locked Ti: sapphire laser (w) which was pumped by Ar^+ laser. The wavelength of Ti: sapphire laser is tunable from 700 nm to 900 nm and the pulse width is 200 fs. The repetition rate of the Ti: sapphire laser is 76 MHz whose time interval is 12.5 ns. The PL luminescence spectrum was measured in conjunction with monochromator using gratings whose grooves are 2400 lines/grooves. To direct examine the optical properties of InGaN/GaN MQW LEDs and avoid the absorption of GaN film, the pumping light source was a frequency doubled Ti: sapphire laser operated on 370 nm. And all the samples were placed in the closed-cycle cryostat with a temperature controller ranging from 20 K to room temperature.

3.4 Low temperature electroluminescence (LTEL)

A set of instruments including current source Kiethley 238, a microscope to

observe the patterned electrode of sample surface, three axial stages for probe and

fiber to detected the light output, and a cryostat for the cooling system which use the

liquid helium to cooling the chamber. Then, the light detected by a 0.32 m

monochromator (Jobin-Yvon Triax-320) with 1800, 1200, and 300 grooves/mm

grating and the maximum width if the entrance slit was 1 mm. And all the samples

were placed in the closed-cycle cryostat with a temperature controller ranging from 77

K (Liquid helium) to room temperature. Fig. 3.4.1 shows the schematic of low

temperature electroluminescence.

p-GaN (200Å)
p-Al$_{0.5}$Ga$_{0.95}$N (500Å)
p-AlGaN EBL (200Å)

InGaN(25Å)/GaN(130Å) MQW

n-GaN : 2.5μm
u-GaN : 1.5μm

Sapphire
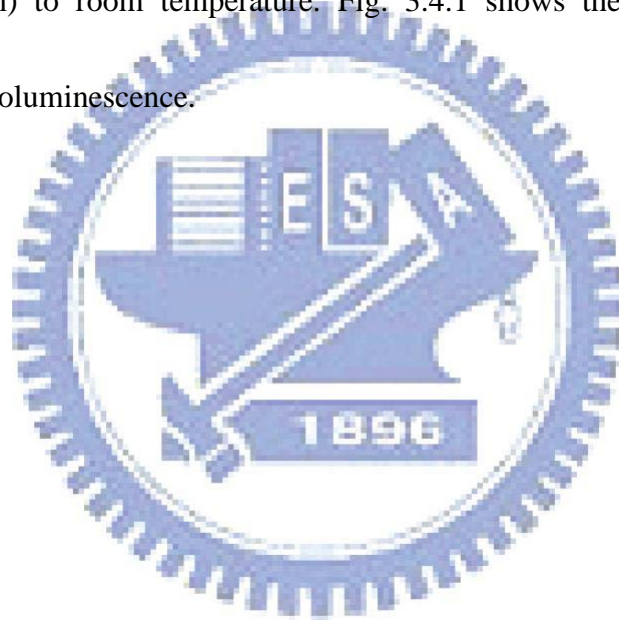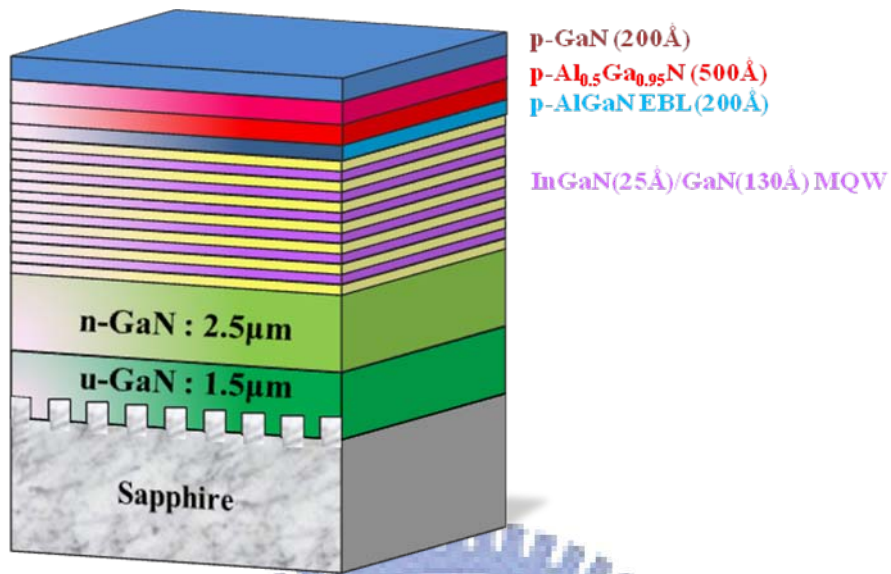
Fig. 3.1.1 The schematic drawing of sample structure

p-GaN
MQWs
n-GaN
u-GaN

Sapphire

Mesa

p-GaN
MQWs
n-GaN

Sapphire

ITO

TCL

Sapphire

Electrode

p-electrode

ITO

p-GaN
MQWs
n-GaN
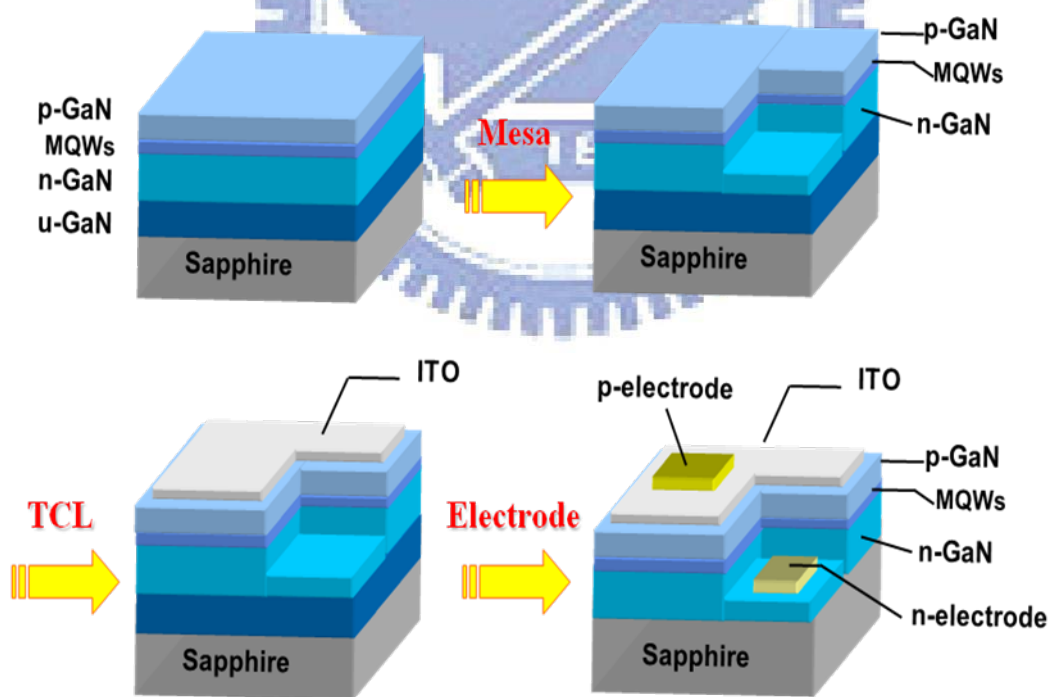n-electrode

Sapphire

Fig. 3.1.2 The schematic drawing of fabrication processes of UV LED
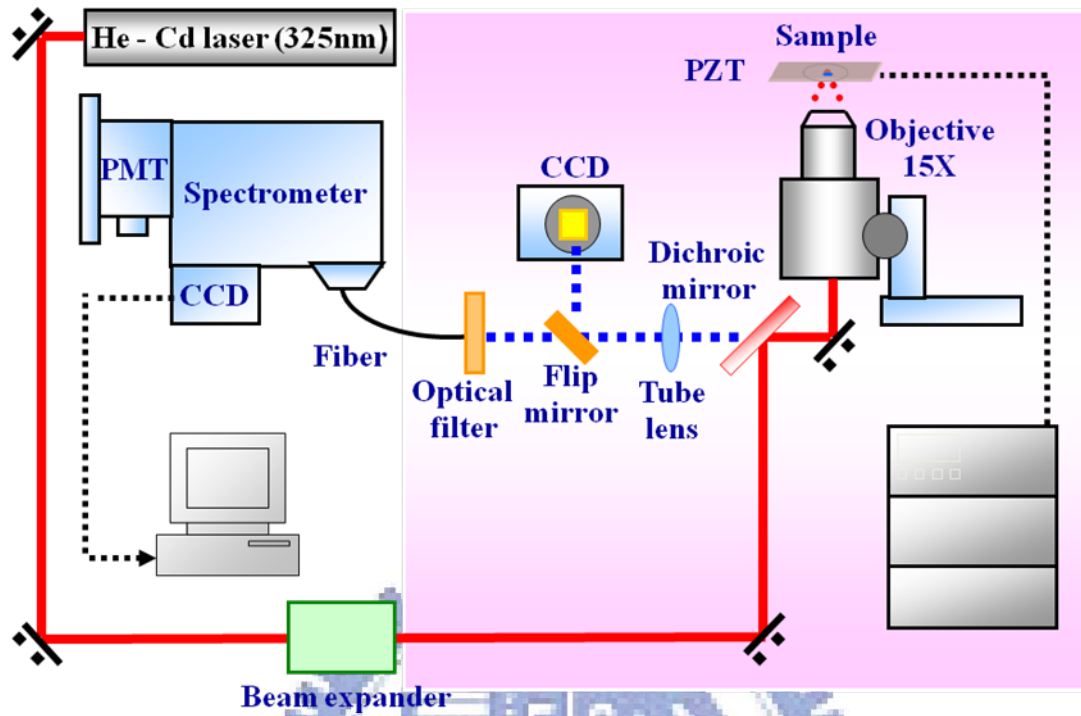
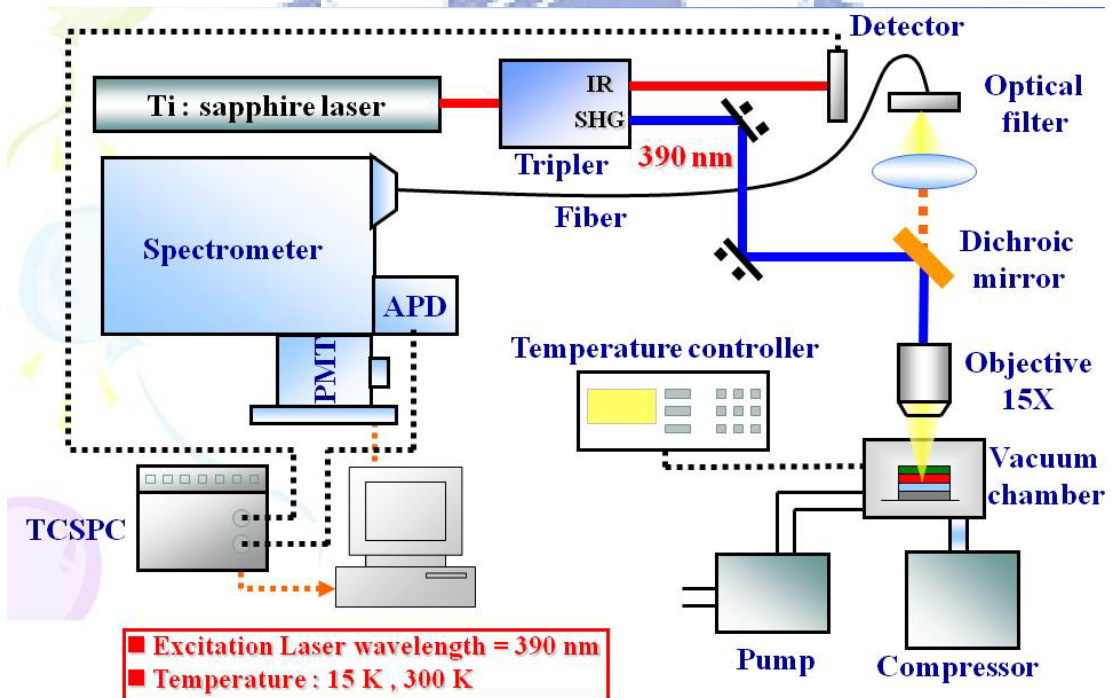Fig. 3.2.1 The schematic of experimental Photoluminescence setup

Fig. 3.3.1 The schematic of IQE measurement system
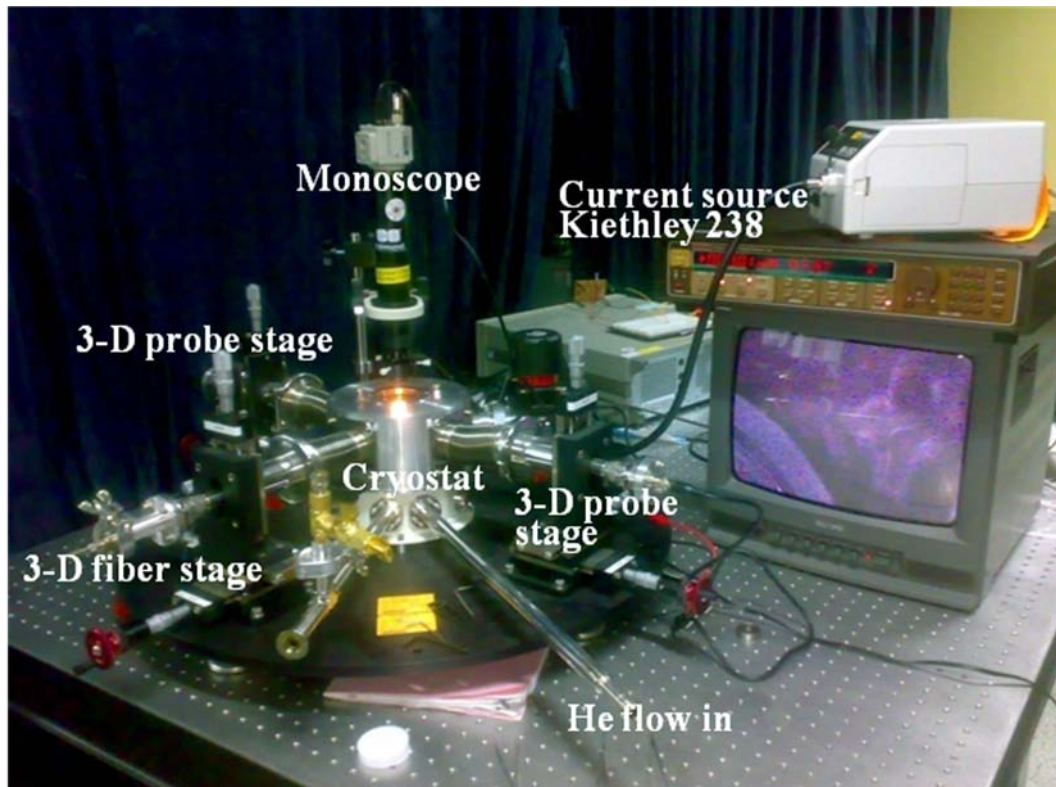
Fig. 3.4.1 The schematic of low temperature electroluminescence

Chapter 4 Excitation power dependent and theoretical model of calculation IQE in InGaN/GaN multiple quantum wells grown on patterned sapphire substrate

4.1 Introduction

To improve the performance of InGaN/GaN LEDs, it is very important to know what physical mechanisms affect the IQE in this material system. Traditionally , the IQE can be obtained by measuring temperature dependent PL at a certain excitation condition, and assume IQE is equal to 100 % at low temperature, then the relative IQE can be obtained at room temperature. However, IQE is well known to be strongly dependent on injected carrier density, especially in $In_xGa_{1-x}N$ MQW system due to the existence of large internal electrical field and potential fluctuation. Therefore, it is important to measure and discuss IQE as a function of excitation power density. It is especially interesting to measure IQE at the carrier density which corresponds to a certain current injection level in EL measurement, for example 20 mA for a small junction chip with conventional size. S. Watanbe et al. [44] proposed a method to determine IQE by performing excitation power density and temperature dependent PL.

In their study, the variation of IQE of InGaN/GaN UV LEDs grown on PSS and conventional substrate with increasing excitation power at 15 K and 300 K has been observed. But they did not say anything more to explain what physical mechanisms occur in it. For this study, we used their calculation method to determine IQE of

InGaN/GaN UV LEDs and also observed that the IQE changes with increasing

excitation power density. Further, we investigated the difference between excitation

power dependence IQE of InGaN/GaN UV LED on PSS and conventional substrate.

The detailed variation of IQE on different substrates will be discussed later.

4.2 The measurement of internal quantum efficiency of InGaN/GaN UV LEDs

For this study, we used the IQE method which S. Watanabe *et al*. proposed to

determine the IQE of InGaN/GaN MQW UV LEDs. The internal quantum efficiency

can be calculated by

$$\eta_{PL} = C \frac{I_{PL} / E_{PL}}{I_{EX} / E_{EX}} \qquad (4.2.1)$$

where I_{PL} and I_{EX} are PL intensity and excitation intensity, respectively. E_{PL} and E_{EX}

are PL photon energy and excitation photon energy, respectively. C is a constant

affected by mostly carrier injection efficiency by laser, light extraction and correction

efficiency of PL, and does not depend on either excitation power density or

measurement temperature. First, we measured the excitation power dependent PL

intensity at low and room temperature, and then the relative PL quantum efficiency

curves can be obtained by using equation 4.2.1. And the constant C would be canceled

out by normalizing the curves to the peak value at the lowest temperature, because it

is independent on temperature or excitation power. From this normalization, the PL

efficiency curves will not depend on carrier injection efficiency by laser, light

extraction and correction efficiency of PL. Therefore, the PL efficiency would be find

out from this model.

In tradition, the IQE is estimated by assuming that IQE is 100 % at low

temperature regardless of excitation power density. However, IQE is strongly

dependent on injected carrier density. Consequently, it is more reasonable to assume

the peak of PL efficiency at lowest temperature is equal 100 %, and then the IQE

curves as a function of excitation power and temperature can be understand.

Moreover, to avoid the absorption of GaN, the frequency doubled femtosecond

pulse Ti: sapphire laser of 370 nm was used to excite sample, the excitation power

density was changed from 0.01 to 15 mW, and calculated injection carrier density is

about 2.0×10^{15} to 1.6×10^{18} cm^{-3} by using the equation below:

$$carrier\ density = \frac{P}{(h\nu)*\phi*d_{active}*f}*\exp(-\alpha_{GaN}d_{GaN})*(1-\exp(-\alpha_{InGaN}d_{active}))R*loss_{objective} \quad (4.2.2)$$

where P is excitation power, hν is energy of incident light, φ is laser spot size, f is

repetition rate of laser, d_{active} is the active layer thickness, α_{GaN} is the   absorption of

GaN, α_{InGaN} is absorption of InGaN, R is reflection of sample surface, and Loss$_{objective}$

is transmission loss of objective.

Fig. 4.2.1 shows the IQE of InGaN/GaN MQW UV LEDs as a function of injected carrier density at 15K and 300 K. We can observe that the IQE increases with increasing injected carrier density to reach its maximum. As injected carrier density further increases, then the IQE decreases. The tendency of two efficiency curves at 15 K and 300 K is very similar. But under low injected carrier density region, the IQE curve at 300 K increases obviously than it at 15 K. The results indicated that the IQE at 15 K saturated more easily than it at 300 K. The detailed physical mechanisms will be discussed later.

There are three possible mechanisms to explain excitation power dependence the IQE at low and room temperature:

(1) Nonradiative recombination centers

For GaN based LED, a large number of dislocation density exist in the device, and the defects would be occurred nonradiative recombination. Generally, the nonradiative centers were quenched at low temperature. In our case, as injected carriers increase, the nonradiative recombination is gradually suppressed, therefore, the radiative recombination stars to dominate the recombination process, resulting in the enhancement of IQE, which is observed in Fig 4.2.1. And IQE curve at 15 K increases not obviously than it at 300 K due to noradiative centers were quenched at low temperature. In Fig. 4.2.1, we found that the IQE of InGaN/GaN UV LED on PSS

27

saturated at lower injected carrier density due to the reduction of carriers captured by

nonradiative recombination centers. The results demonstrated that InGaN/GaN UV

LEDs on PSS has better crystal quality and smaller defect density.

(2)   Coulomb screening effect

Several research groups have reported that the internal electric field existed in

InGaN/GaN QW structure. This internal electric field through the QW tilts the

potential band and leads to a spatial separation of electrons and holes in the QW [45],

resulting a decreasing in degreed of wave function overlap which is called the QCSE.

The internal electric filed in the QW cam be screened by photogenerated carriers.

Consequently, the QCSE effect become weaker when the carrier density increased,

resulting in the IQE enhanced at low injected carriers region.

(3)   Band filling effect of localized states

Due to composition inhomogeneity and monolayer thickness fluctuation Of

InGaN QWs self-organized In-rich region is generated in InGaN active region,

resulting in potential fluctuation of energy bandgap. As injected carrier density

increases further, an occupation of high energy stats of localized centers will be

enhanced. And the band filling effect will make the carriers more easily escape from

localized states to extendend states which decrease IQE.

The experimental results indicated that the IQE are about 61.0 %, 44.2 % at

injected carrier density is 4.7 $\times$ 10^{17} #/cm^3(~20mA) for InGaN/GaN UV LED on PSS

and conventional substrate, respectively. Table 4.3.1 shows the value of IQE and EQE,

and then we calculated the extraction efficiency using the relation equation:

$$\eta_{EQE} = \eta_{IQE} * \eta_{Extraciotn} .$$ (4.2.1)

We can obtained the extraction efficiency are about 70.5 %, 63.3 % for InGaN/GaN

UV LED on PSS and conventional substrate, respectively. Several research groups

demonstrated PSS can reduce the threading dislocations and increase the light

extraction. Our results also indicated that InGaN/GaN UV LEDs on PSS increase the

IQE (and light extraction efficiency.
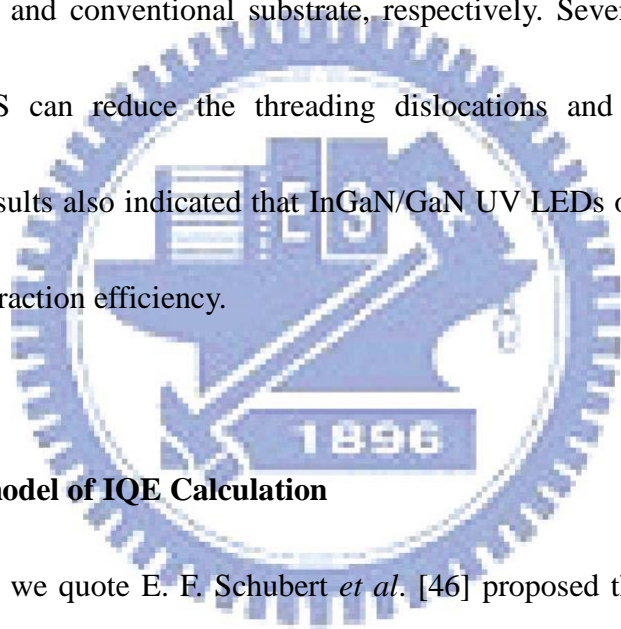
4.3 Theoretical model of IQE Calculation

In this study, we quote E. F. Schubert *et al*. [46] proposed theoretical model to

calculate IQE of InGaN/GaN MQW UV LEDs. The three main carrier-recombination

mechanisms in a bulk semiconductor are Shockley–Read–Hall nonradiative

recombination, expressed as An, bimolecular radiative recombination Bn^2, and Auger

nonradiative recombination Cn^3, where A, B, and C are the respective recombination

coefficients and n is the carrier concentration. Auger recombination affects LED

efficiency only at very high excitation; thus, in our experiments, the generation rate

and the IQE at steady state can be expressed as

$$G = R_{total} = An + Bn^2 + Cn^3 \tag{4.3.1}$$

$$IQE = \frac{Bn^2}{An + Bn^2} = \frac{Bn^2}{G} \tag{4.3.2}$$

and the integrated PL intensity can be expressed as

$$I_{PL} = \eta Bn^2 \tag{4.3.3}$$

where η is a constant determined by the volume of the excited active region and the total collection efficiency of luminescence. By eliminating n in equation 4.3.1 and 4.3.3, we can express the generation rate in terms of integrated PL intensity

$$G = \frac{A}{\sqrt{B\eta}}\sqrt{I_{PL}} + \frac{1}{\eta}I_{PL} + \frac{C}{(B\eta)^{1.5}}I_{PL}^{1.5} \tag{4.3.4}$$

$$G = P_1\sqrt{I_{PL}} + P_2 I_{PL} + P_3 I_{PL}^{1.5} \tag{4.3.5}$$

$$IQE = \frac{Bn^2}{G} = \frac{I_{PL}}{\eta G} = \frac{I_{PL}P_2}{G} \tag{4.3.6}$$

The connection between theory and experiment is completed by noting that the generation rate can be separately calculated from experimental parameters using

$$G = \frac{P_{Laser}(1-R)\alpha l}{A_{spot}lh\nu} = \frac{P_{Laser}(1-R)\alpha}{A_{spot}h\nu} \tag{4.3.7}$$

where P_{Laser} is the peak optical power incident on the sample, R (18 %) is the Fresnel

reflection at the sample surface, l (15 nm) is the total thickness of the InGaN QWs,

A_{spot} (1.96 × 10³ μ m²) is the area of the laser spot on the sample surface, $h\upsilon$ (3.18

eV) is the energy of a 370 nm photon, and. α m⁻¹) is the absorption coefficient of the

$In_{0.1}Ga_{0.9}N$ well at 370 nm.

First, we measured the PL spectrum dependent excitation power, and then the

generation rate (G) curves as a function of PL intensity (I_{PL}) can be obtained by using

equation 4.3.4. We used equation 4.3.4 to fit the experimental data in Fig. 4.3.1, then

we obtained the coefficients $P_1 = A(B\eta)^{0.5}$, $P_2 = 1/\eta$, $P_3 = C/(\eta B)^{1.5}$. The fitting curves

appear to accurately model our experiments, also shown in Fig. 4.2.1. If one assumes

a value of B at room temperature of 1 × 10⁻¹⁰ cm³/s, the value of carrier

concentration n can also be obtained. By eliminating η from the two coefficients P_1

and P_2, one can obtain the value of coefficient A finally. The table 4.3.1 shows the

nonradiative coefficient A at low and room temperature. The nonradiative coefficient

A as a function of dislocation density, including values of 8.66 × 10⁵, 1.64 × 10⁶ at

low temperature and 1.28 × 10⁷, 2.45 × 10⁷ s⁻¹ for InGaN/GaN UV LEDs on PSS

and conventional sapphire substrate, respectively. Nonradiative coefficient of without

PSS UV LED is larger than PSS at low and room temperature. Generally,

threading-dislocation density significantly affects the InGaN MQW efficiency, which

supports the argument that threading dislocations behave as nonradiative

recombination centers. The results indicated the InGaN/GaN UV LEDs on PSS has

better crystal quality and larger quantum efficiency due to the reduction of threading
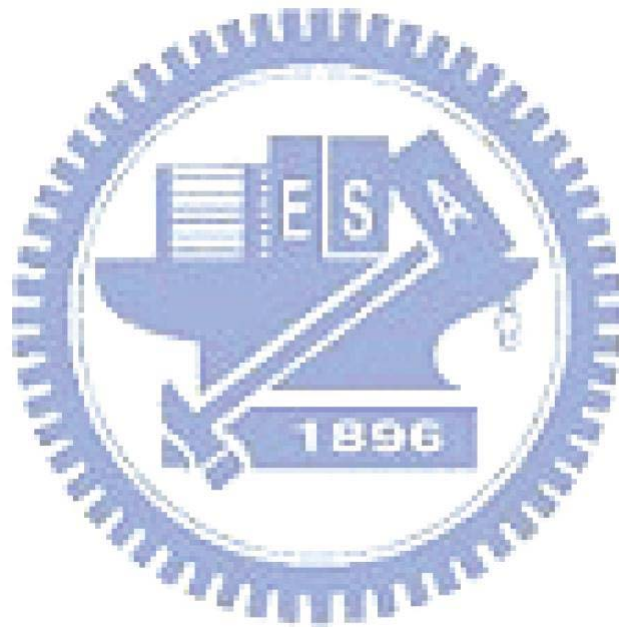
dislocation density.

After that, we know the carrier concentration n and P_2, so we can be obtained

IQE curves as a function of carrier concentration n in Fig 4.3.2. The calculation of

IQE is very similar to our experimental results. Fig. 4.3.3 shows the emission power

as a function of current density, different slopes can be attributed to different terms

dominating the recombination-rate equation.

We can reproduce the dependence of the internal efficiency on current density, J,

using a simple rate-equation model of the form

$$J \sim An + Bn^2 + Cn^3 \qquad\qquad (4.3.8)$$

where n is the QW carrier density and A, B, and C are coefficients for nonradiative,

radiative, and (nonradiative) Auger-like recombination, respectively. We thus identify

a high-density QW-internal Auger-like process as the culprit for the high-current

losses observed, with C = 6.03×10^{-29} and 1.33×10^{-29} cm^6/s for InGaN/GaN UV

LEDs on PSS and conventional substrate at room temperature. The value of C is

higher than the normal Auger coefficient (10^{-30}~10^{-34} cm^6/s). And the calculated order

of carrier density (~ 10^{18} #/cm^3) is not in the typical region of Auger recombination (~

10^{19} #/cm^3). The hole mobility decreased at low temperature resulting in hole couldn't

transport to the later QW effectively. The results indicated that the carrier distribution

is not uniform in the QW; the carrier density may be attained ~10^{19} #/cm^3 to occur

Auger-like recombination in some QW. Therefore, we demonstrated the Auger-like

effect affect the efficiency droops at high injection current. The efficiency droop may
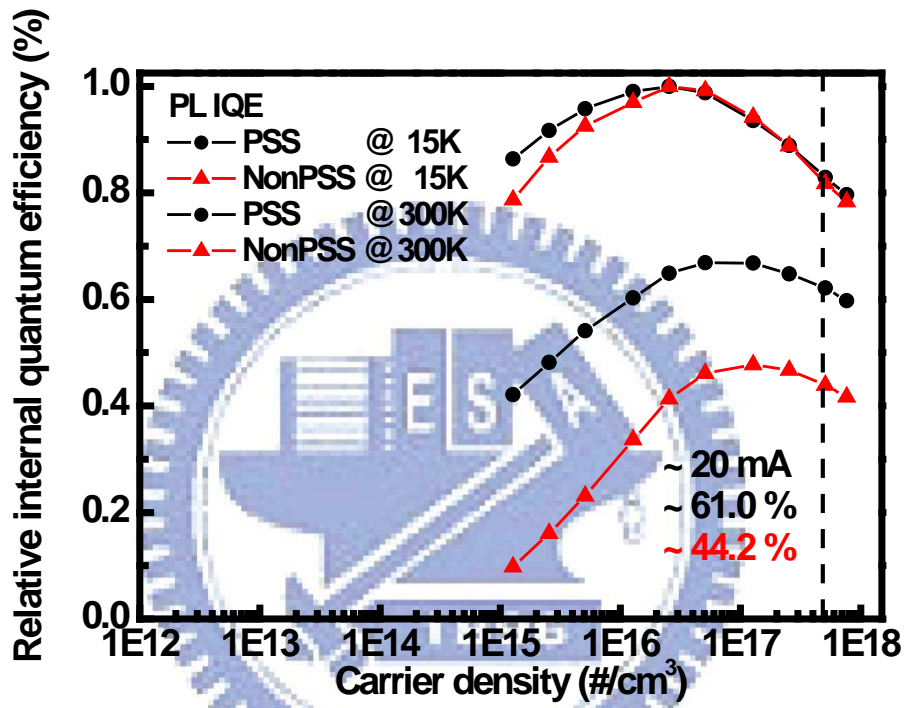
be dependent on Auger-like effect.

Fig 4.2.1 IQE of InGaN/GaN LEDs as a function of carrier density at 15K and 300 K.
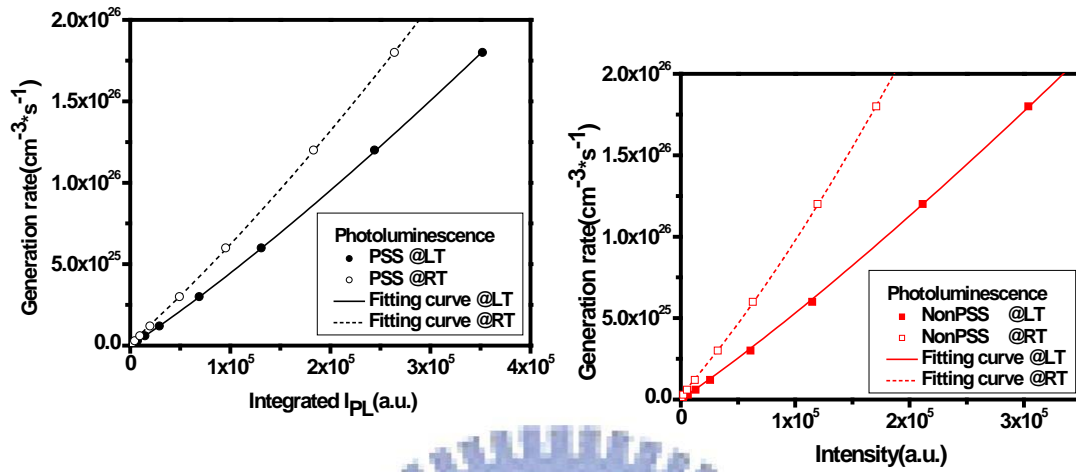
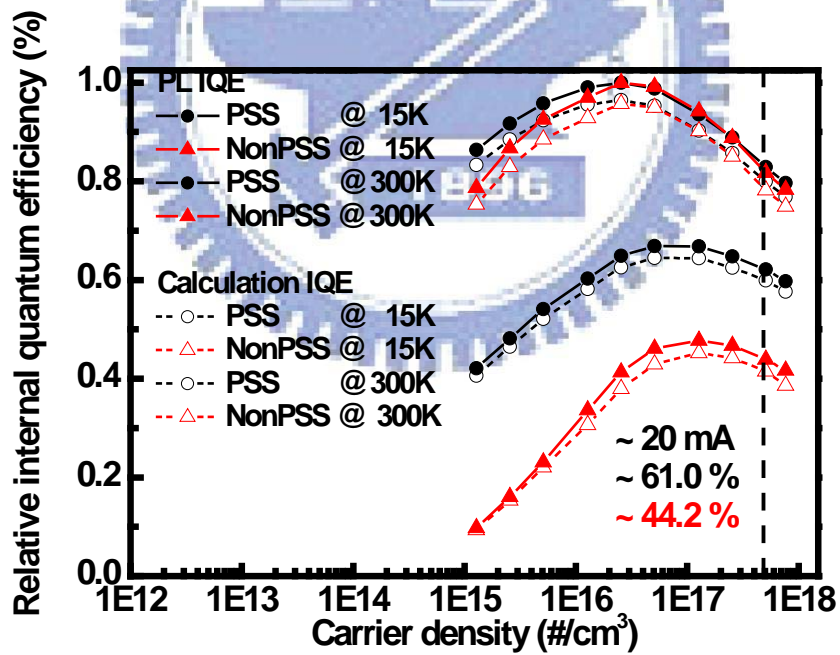Fig. 4.3.1 Generation rate G as a function of integrated PL intensity (I_{PL})

Fig. 4.3.2 Internal quantum efficiency as a function of carrier concentration n
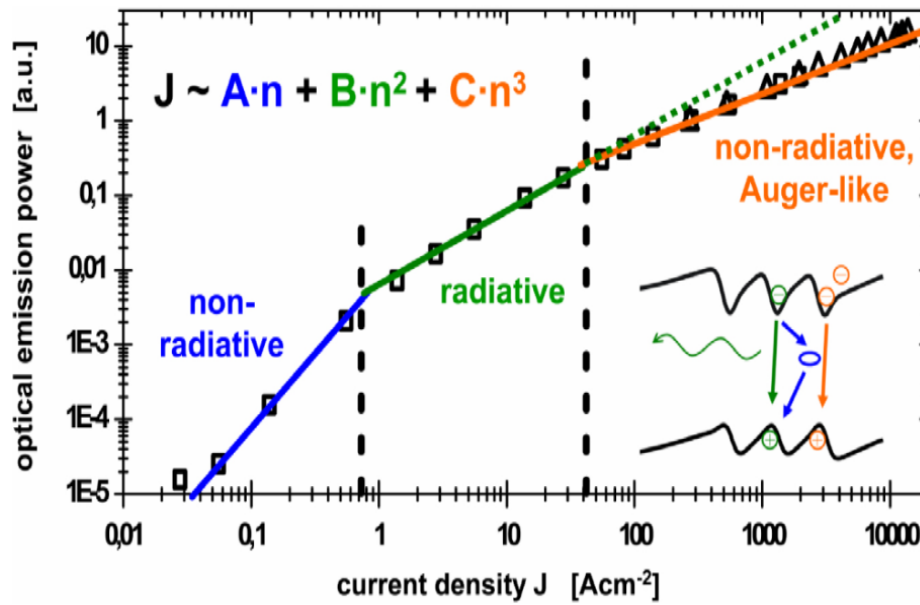
Fig. 4.3.3. Emission power as a function of current density, different slopes can be attributed to different terms dominating the recombination-rate equation
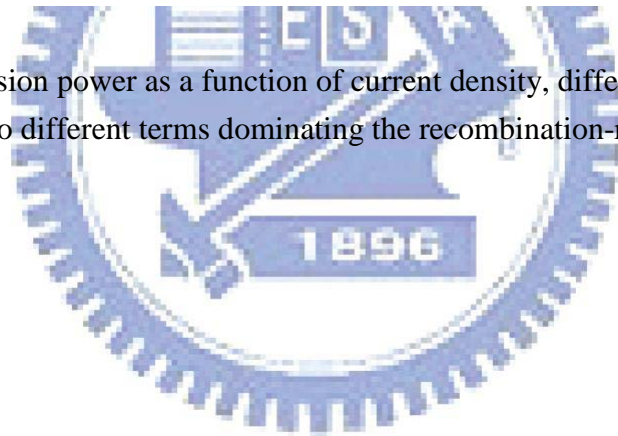
Table 4.2.1 Efficiency parameters on PSS and without PSS InGaN/GaN UV LED

Sample	PL IQE (%)	Exp. EQE (%)	Extraction (%)
PSS	~ 61.0%	~43.0%	~70.5%
NonPSS	~ 44.2 %	~28.0%	~63.3%

Table 4.3.1 Nonradiative coefficient *A* from fitting equation 4.3.4

Sample	$A\ (s^{-1})$ @ 15K	$A\ (s^{-1})$ @ 300 K
PSS	8.66×10^5	1.28×10^7
NonPSS	1.64×10^6	2.45×10^7

Table 4.3.2 Experimental IQE and calculation IQE

Sample	PL IQE (%)		Calculation of IQE (%)	
	15K	300 K	15K	300 K
PSS	~85.9 %	~61.0%	~82.4 %	60.6%
Non-PSS	~85.9%	~44.2%	~82.4%	41.8%

Table 4.3.3 Auger coefficient calculation and normal *C*: $10^{-30} \sim 10^{-34}$ cm^6/s

Sample	$C\ (cm^6/s)$ @LT	$C\ (cm^6/s)$ @RT
PSS	2.48×10^{-29}	6.03×10^{-29}
NonPSS	3.02×10^{-29}	1.33×10^{-28}

Chapter 5 Analysis of electroluminescence and efficiency droop in InGaN/GaN multiple quantum wells grown on patterned sapphire substrate

5.1 Introduction

Recently some research groups have investigated temperature dependence of the electroluminescence (EL) spectral intensity [47][48][49], which reveals anomalous EL quenching at lower temperatures below 100 K. It is found that the anomalous temperature dependence of the EL efficiency is caused by interplay of the carrier capture and the IQE. One interesting observation of the InGaN/GaN QW diodes so far is that the EL efficiency dramatically decreases when the diode temperature is decreased below 100 K, where the improved EL efficiency is generally expected due to the decreased nonradiative recombination processes. One of the anticipated genuine causes for the low temperature EL quenching may be ascribed to the deep Mg acceptor level of 170 meV in *p*-GaN [50], which can be deactivated at lower temperatures below 100 K. Therefore, holes are failed to be injected into the QW active region from the *p*-GaN layer, especially when the electron blocking *p*-type AlGaN barrier is introduced. For this study, detailed physical mechanisms for the EL enhancement effects under the forward bias conditions have been confirmed. And we have investigated the carrier transport mechanisms particularly by using APSYS simulation.

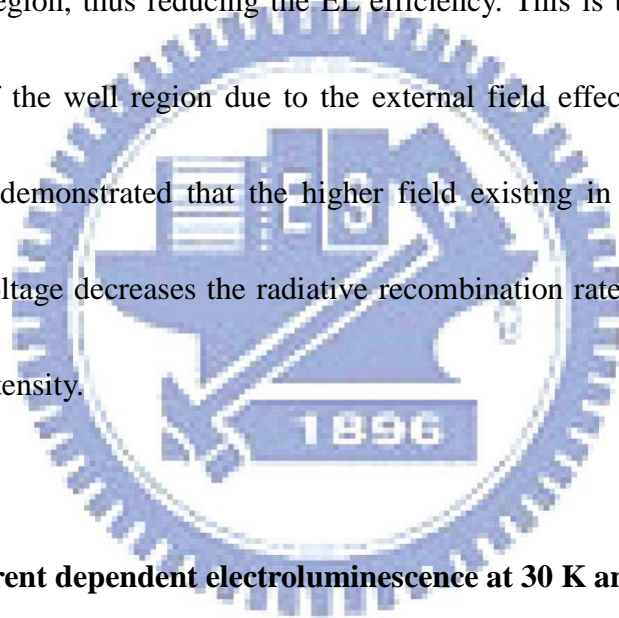**5.2 Temperature dependent electroluminescence**

Temperature dependence of the EL spectra at various injection current levels has been measured between 30 and 300 K. Three-dimensional (3D) plots of the EL results at three injection currents of 0.1, 1, and 20 mA are shown in Figs. 5.2.2 (a)-(c), respectively. First, at the lowest current of 0.1 mA in Fig. 5.2.2(a), the EL intensity shows the highest value at the lowest temperature of 30 K. This result is interpreted as showing the EL efficiency basically determined by the nonradiative recombination centers at low injection current. We can observe the EL intensity decrease slightly from 300 K to 30 K when injection current is 1 mA. When temperature is slightly decreased from 300 K to 100 K at 20 mA, the EL spectral intensity efficiently increases, and reaches the maximum around 100 K. However, with further decrease of temperature down to 15 K, significant reduction of the EL intensity is observed. We will be discussed the detailed physical mechanisms later.

In order to check the EL efficiency, the relative EL efficiency is plotted as a function of temperature in Fig. 5.2.3 and Fig. 5.2.6 at injection currents of 0.1, and 20 mA. Generally, thermal quenching phenomenon was observed in InGaN-based structures. At low injection current, the carrier injected into quantum well, and then the carriers can be confined due to the localized states in the In-rich region. In InGaN-based structures, the emission came from the localized states, which could trap

carriers within this potential minimum. Fig. 5.2.5 shows the schematic drawing of effective localized states and defect states. When the temperature increased, the carrier could receive activation energy to thermalize from radiative or/and localized centers to nonradiative or/and delocalizaed centers resulting in the EL efficiency decreased. When temperature decreased, the forward voltage increased of InGaN/GaN UV LEDs due to the hole concentrations and mobility decreased [51]. But we observed the forward voltage change slightly at low injection current that indicated it didn't affect the EL efficiency seriously in Fig 5.2.4 (b). Fig. 5.2.7 (b) shows the temperature dependence forward voltage, we found that the EL efficiency decreased while decreased temperature from 100 K to 30 K. There are two possible mechanisms interplay with increasing temperature, and then the EL efficiency is affected by carriers escape from localized states into defect states of low injection current at 0.1 mA. But the temperature dependence EL efficiency at 20 mA decreased when further decreasing temperature, the results can be attributed to the forward voltage increased rapidly due to the hole concentrations and mobility decreased.

A reduction of the EL intensity is clearly seen with decreasing the temperature below 80 K after reaching the maximum EL intensity around 100 K at 20 mA. In Fig 5.2.7 (b), the forward voltage increased about 1 and 1.4 V for InGaN/GaN UV LEDs on PSS and conventional substrate, respectively. Therefore, we conclude that the

variation of V_f plays an important role in temperature dependence EL efficiency, especially, the EL efficiency may be affected when decreasing temperature at high injection current. In high injection current, it appears that the carriers are effectively captured by active centers in the MQW under the application of lower forward voltage at room temperature. But, forward voltage increased while decreasing temperature, they are rather transferred to nonradiative recombination centers as a result of escape from the MQW region, thus reducing the EL efficiency. This is because the carriers can escape out of the well region due to the external field effects in high injection current. We also demonstrated that the higher field existing in the well under the higher forward voltage decreases the radiative recombination rate, which also causes the reduced EL intensity.

5.3 Injection current dependent electroluminescence at 30 K and 300 K

In order to show detailed variations of the EL efficiency as a function of injection current at various temperatures, the integrated EL intensity divided by current, which is proportional to the EL quantum efficiency, is plotted in Fig 5.3.1 and Fig. 5.3.3 as a function of logarithmic current at 30 K and 300 K. The EL quantum efficiency at 30 K increased slightly with increasing injection current due to injected carrier attributed to compensate the nonradiative recombination centers, and reaches the maximum at

about 1mA. We can observe the EL quantum efficiency at 0.1 mA of InGaN/GaN UV LED on PSS is higher than conventional sapphire substrate, and then the EL quantum efficiency reaches the maximum at lower injected current. The results demonstrated the slight variation of EL quantum efficiency due to the reduction of dislocation density of InGaN/GaN UV LED on PSS. While further increasing injection current, the EL efficiency droops rapidly, we observed that the reduction of EL efficiency of InGaN/GaN UV LED on PSS is very similar to conventional sapphire substrate. The results indicated that the reduction of dislocation density didn't affect the efficiency droop at high injection current. Fig. 5.3.2 shows the schematic drawing of current dependence EL efficiency. While further increasing injection current, the EL quantum efficiency deceased rapidly which the forward voltage drastically increased at 30 K which show in Fig. 5.3.2 (b). We attribute this reduction of EL quantum efficiency at high injection currents to the higher forward voltage which resulting in carriers escape from the quantum well and overflow to p-GaN.

Fig 5.3.3 display the EL quantum efficiency increased obviously with increasing injection current at 300 K, since the nonradiative recombination centers are partially activated at higher temperature. In Fig 5.3.4 (a), we can see the schematic drawing of current dependence EL efficiency at 300 K. Identically, we found that the EL quantum efficiency of InGaN/GaN UV LED on PSS is higher than conventional sapphire

substrate. And the EL efficiency droops more slightly at 300 K with further increasing

injection current, which can be ascribed to the reduction of forward voltage at high

injection current that show in Fig 5.3.4 (b).

5.4 Analysis of injection carrier density dependence EL efficiency and efficiency droop

Fig 5.4.2 and 5.4.3 show the temperature dependent EL efficiency as a function

of injection current of InGaN/GaN UV LED on PSS and conventional sapphire

substrate, respectively. We use Shuji Nakamura and Steven P. Denbaars et al. [52]

proposed equivalent circuit model (should add the model and explain what it means

for) to explain the temperature dependence EL efficiency as a function of injection

current. These four components are put in an equivalent circuit model illustrated in

Fig. 5.4.1 (a). This circuit model ensures all injected carriers are traced and are not

unintentionally lost. The resistor R_1 represents current leakage paths, such as extended

crystal defects) and sample surface) For example. This current component is not

considered to involve carrier recombination, hence is purely carried by electrons.

There are two diodes. Diode D_1 is responsible for current flow due to radiative

recombination. This current component results in photon emission and detection upon

recombination. Diode D_2 is responsible for nonradiative recombination current. Such

recombination occurs via nonradiative recombination centers (NRCs) and does not

emit photons within the wavelength range of interest. These two types of recombination are not limited within or near the active region. They are distinguished by whether a photon is emitted and detected within the wavelength range of interest upon a recombination event. Another resistor R_2 combined with a switch represents carrier overflow. This component is considered to be the electron unipolar current, i.e., is carried by electrons that do not recombine with holes and exit the system to the p-type contact. Current division between I_{D1} (through D_1) and I_{D2} (through D_2) is defined as:

$$\beta = \frac{I_{D1}}{I_{D1} + I_{D2}} = \frac{r_R}{r_R + r_{NR}} \qquad (5.4.1)$$

where r_R is the radiative recombination rate and r_{NR} is the nonradiative recombination rate. EL efficiency is defined in this current range as

$$\eta = \frac{I_{D1}}{I_T} = \beta \frac{I_D}{I_T} \qquad (5.4.2)$$

where $I_D = I_{D1} + I_{D2}$ and $I_T = I_D + I_{R1}$ have been implemented. Ohms law and the diode equation are taken to identify the fundamental behavior of:

$$I_{R1} = \frac{V}{R_1} \qquad (5.4.3)$$

$$I_D = I_{D0}\left[\exp\left(\frac{qV}{nkT}\right) - 1\right] \qquad (5.4.4)$$

V is the applied voltage, I_{D0} is the diode saturation current, q is the unit charge, n is

the ideality factor, k is the Boltzmann constant, and T is the absolute temperature.

Equations (5.4.3) and (5.4.4) can be related via V to obtain from eq. (5.4.2) as

$$\eta = \beta(T)\left[\frac{1}{I_D}\frac{nkT}{qR_1}\ln\left(\frac{I_D}{I_{D0}} + 1\right) + 1\right]^{-1} \tag{5.4.5}$$

Figure 5.4.1 (b) is going to be compared to experimental results. We can observe

the entire curve gradually shifts upwards towards EL efficiency ~ 1 as a result of

nonradiative recombination centers deactivation when temperature is reduced. In this

model, the EL efficiency increased when increasing injection current, and the EL

efficiency curve bending less sharp while temperature is decreasing. The phenomenon

indicated that the significant leakage current existed, and the leakage current is

reduced when temperature decreased.

Fig. 5.4.3 shows the EL efficiency as a function of injection current at 77 K and

300 K, and the EL efficiency are 60.3 %, and 41.6 % at 20 mA of InGaN/GaN UV

LED on PSS and conventional sapphire substrate, respectively. The EL results is

similar to the PL efficiency which show in table 5.4.2, therefore, we also can obtained

the internal quantum efficiency by temperature dependence EL measurement.

5.5 Comparison of PL and EL efficiency

Fig. 5.5.1 displays the PL efficiency and EL efficiency as a function of carrier density at low and room temperature. We can observe that the PL efficiency is higher than EL efficiency at low carrier density, the results indicated that more leakage current occurred when carrier injected into quantum well due to the injected carriers may be captured by nonradiative recombination centers in n-GaN when using current source. Fig. 5.5.2 (a) demonstrated that some leakage current appeared in n-GaN, but when using 370 nm laser to excited carrier which electron and hole pairs occurred in multiple quantum well without absorption of n-GaN. Further increasing injected carrier density, the PL and EL efficiency decreased due to carrier overflow from quantum well which show in Fig. 5.5.2 (b). And we found that the EL efficiency decreased more rapidly at high injected carrier density, it can be attributed to the forward voltage increased when increasing injected carrier density. The results demonstrated that carriers escape from the quantum well and overflow to p-GaN. Fig. 5.5.3 indicated more carriers injected to p-GaN at high current which resulting in the efficiency droop more quickly.

Fig. 5.4.3 shows the EL efficiency as a function of .injection current at 77 K and 300 K. We discovered that the EL efficiency droops more rapidly at 77 K that it at 300 K. Fig. 5.5.6 and Fig. 5.4.20 display temperature dependence electron concentration

and mobility and temperature dependence hole concentration and mobility [53],

respectively. From Fig 5.5.6, we observed the electron concentration and mobility

decreased when decreasing temperature, but the electron mobility only a little decayed.

The hole concentration and mobility decreased drastically with decreasing

temperature, the hole mobility have one order decayed. This phenomenon caused that

hole concentration distribution is not uniformly and is insufficient due to the low hole

mobility, therefore, some electrons transport to the later quantum well near *p*-GaN

when electron injected into quantum well. And these injected electrons further reach

the *p*-GaN resulting in the EL efficiency droop more rapidly at 77 K than 300 K. The

Schematic drawing of electron and hole concentration distribution at low and high

injection current which show in Fig. 5.5.5.
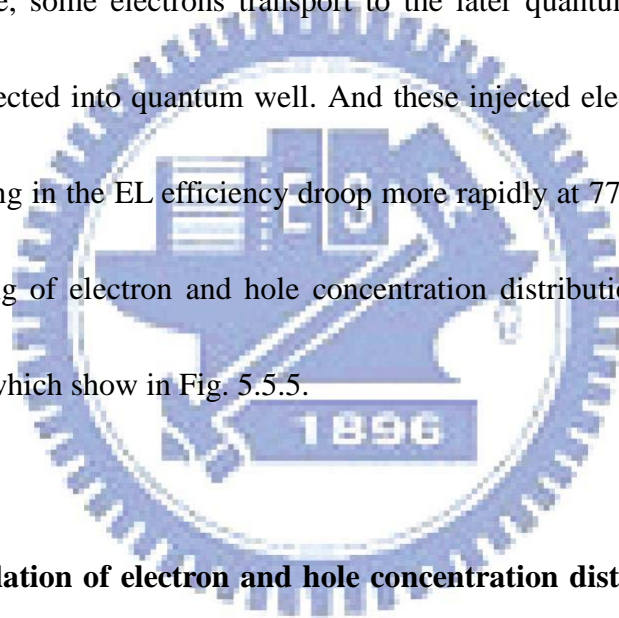
5.6 APSYS simulation of electron and hole concentration distribution and band

    diagram at high injection current

We wanted to know the carrier concentrations distribution under high injection

current at low and room temperature; therefore, we use APSYS to simulate our

sample structure. Fig. 5.6.1 shows the simulation of I-V curve with different hole

concentration and mobility. The solid line represents our experimental results and the

dash line represents the simulation results, we tried to change the parameters of hole

concentration and mobility to coincide with our experimental results. We can see the simulation of I-V curve is similar to experimental results. Further, Fig. 5.6.2 (a) show the electron concentration distribution in multiple quantum well, the black and red line represents the condition at 300 K and 77 K, respectively. The electron concentration distribution is uniform in the QW, but we can observe the electron concentration in QW near the p-GaN is higher (~five times) than near n-GaN, the results demonstrated that some electrons transport to p-GaN which just like the contention we mentioned above. Fig. 5.6.2 (b) displays the hole concentration distribution in MQW, we found the hole concentration is not uniform in the QW, the hole concentration in QW near p-GaN is higher (~ one order) than near n-GaN. The hole concentration distribution is not uniform which can be attributed to the hole mobility decreased at low temperature resulting in hole couldn't transport to the later QW effectively. Under this condition where thermal generation of holes is insufficient and injected electrons continuously deplete holes, some of the injected electrons reach the p-GaN and exit the system without being able to recombine. Then, Fig. 5.6.3 shows the radiative recombination rate of each quantum well, we observed that the readiative recombination rate is higher near p-GaN which indicated the hole is insufficient to supply the radiative recombination of QW near n-GaN. Consequently, the results verified the EL efficiency droop more rapidly at lower temperature.
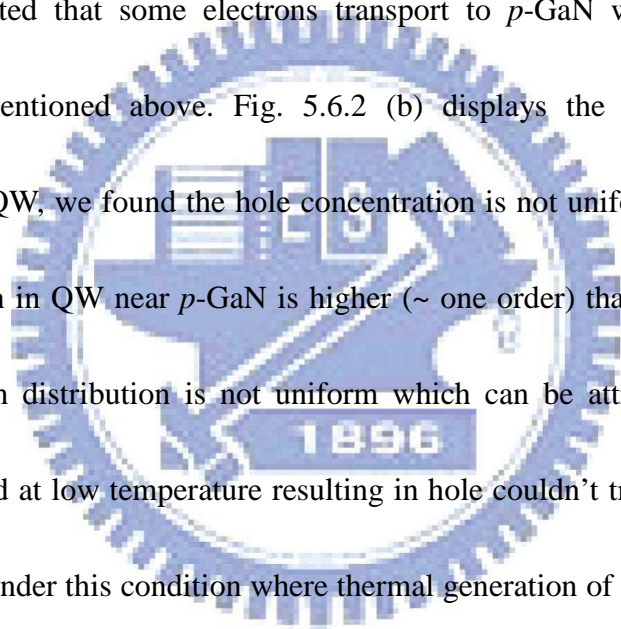
Finally, Fig. 5.6.4 shows the band diagram at high injection current of InGaN/GaN MQW at low and room temperature. From this picture, high forward voltages for significant currents to flow, so that the conduction band on the *n*-side of the device is significantly higher than the conduction band on the *p*-side. This makes it energetically favorable for electrons to escape to the *p*-side of the device. The band inclined caused that more carriers overflow from quantum well and transport to *p*-GaN, the results make the EL efficiency droop quickly at lower temperature.
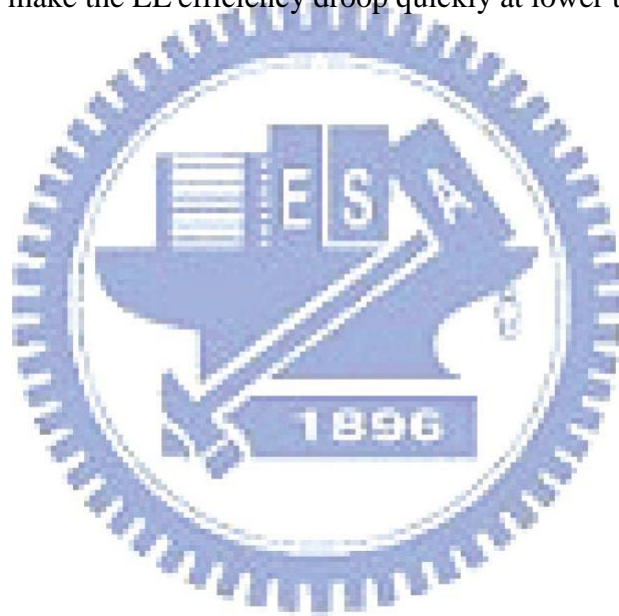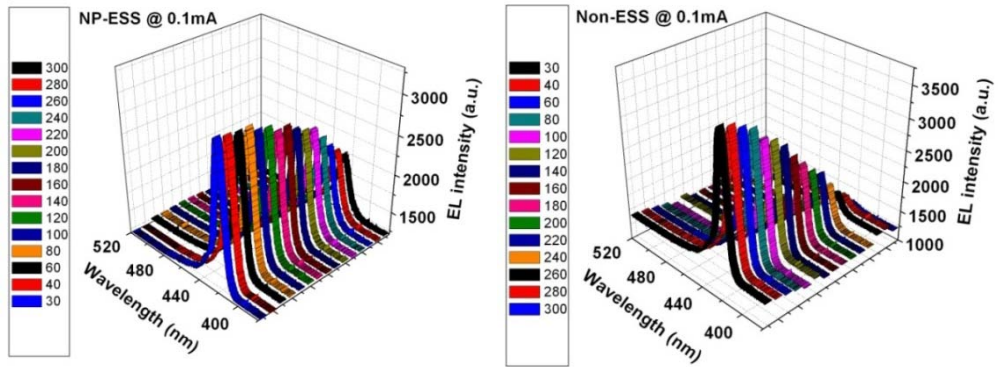
Injection current 0.1mA
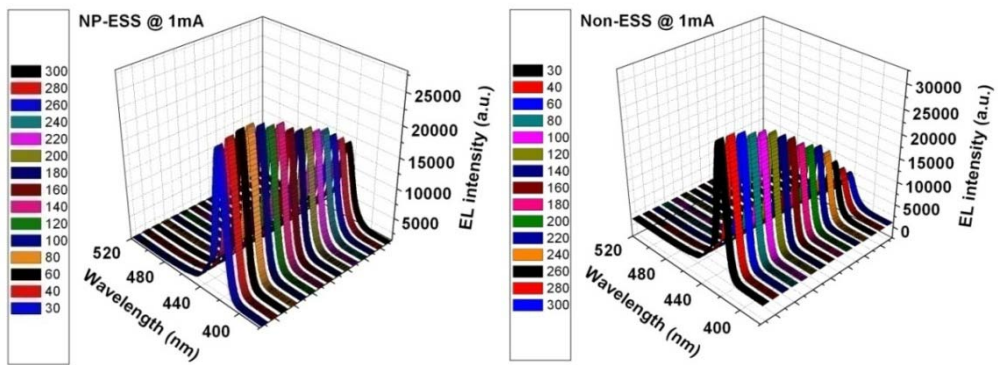
Injection current 1mA
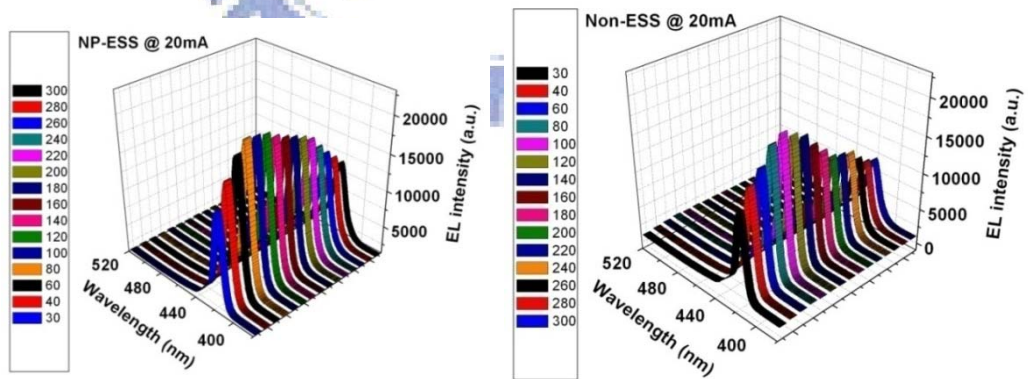
Injection current 20mA

Fig. 5.2.2 Temperature dependence of the EL spectra for InGaN/GaN UV LED at

injection currents of (a) 0.1 mA, (b) 1 mA, and(c) 20 mA.
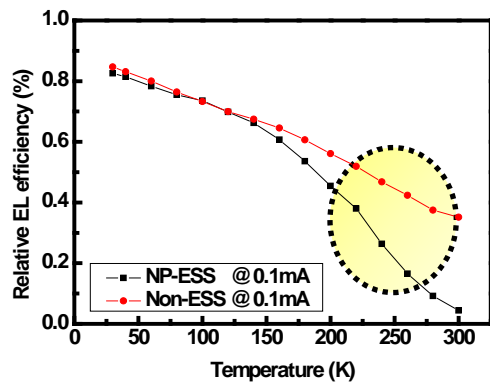
Fig. 5.2.3 Temperature dependence of the EL efficiency at 0.1mA

(a)   (b)
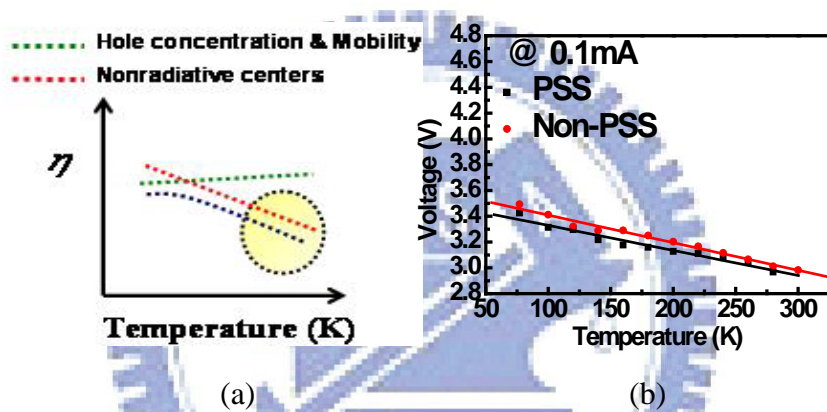
Fig. 5.2.4 (a) Schematic drawing of temperature dependence EL efficiency
(b) Temperature dependence forward voltage at 0.1mA
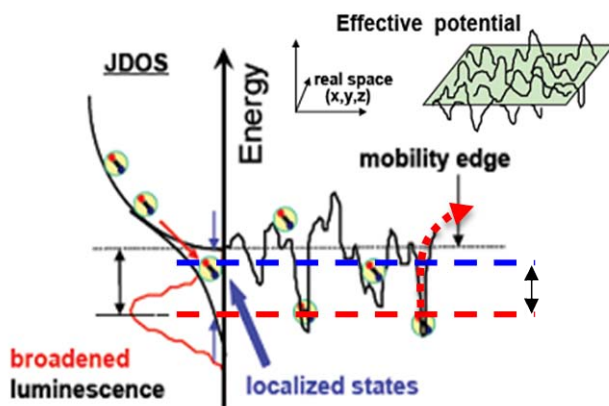
Fig. 5.2.5 Schematic drawing of effective localized states and defect states

51
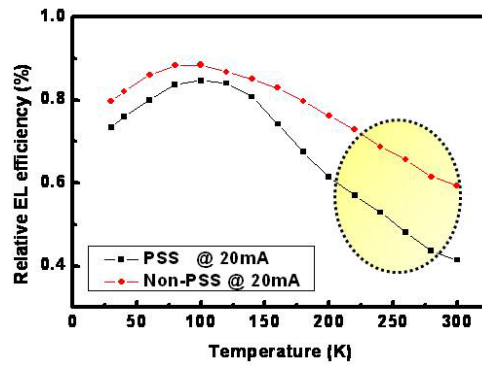
Fig. 5.2.6 Temperature dependence of the EL efficiency at 20mA

(a)   (b)
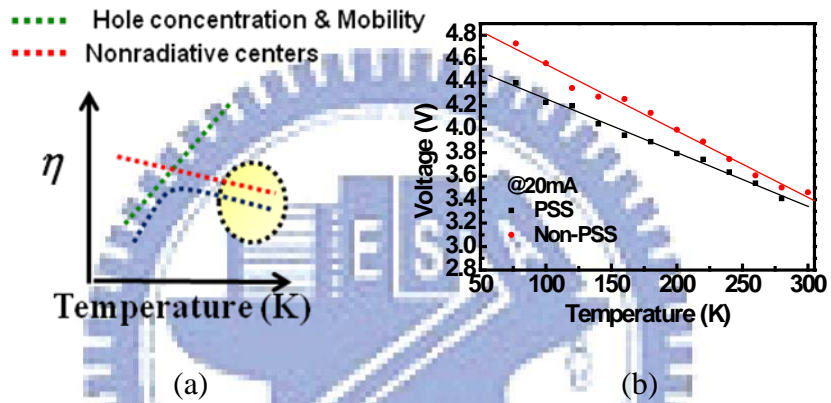
Fig. 5.2.7 (a) Schematic drawing of temperature dependence EL efficiency
(b) Temperature dependence forward voltage at 20mA
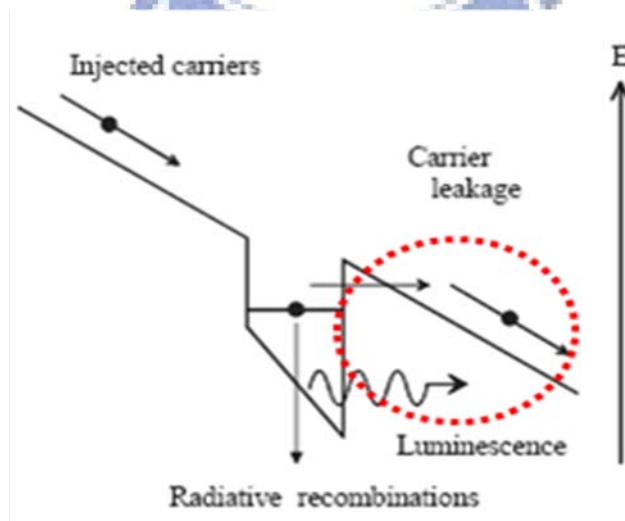
Fig. 5.2.8 Schematic model for carrier capturing influenced under higher voltage
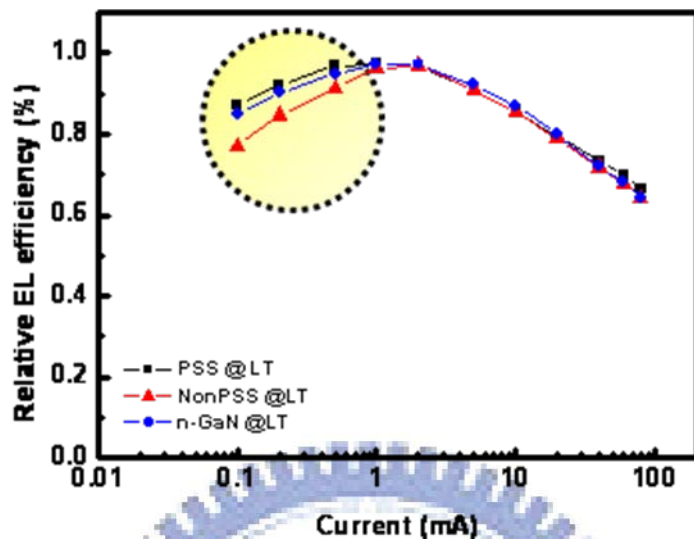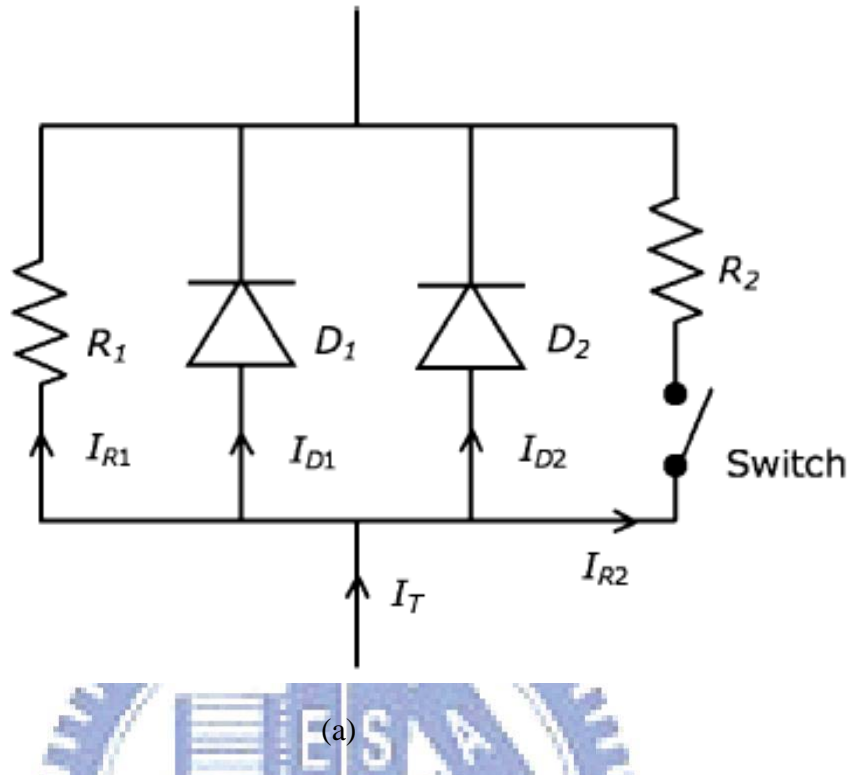
Fig. 5.3.1 Current dependence of the EL efficiency at 30K

(a)   (b)
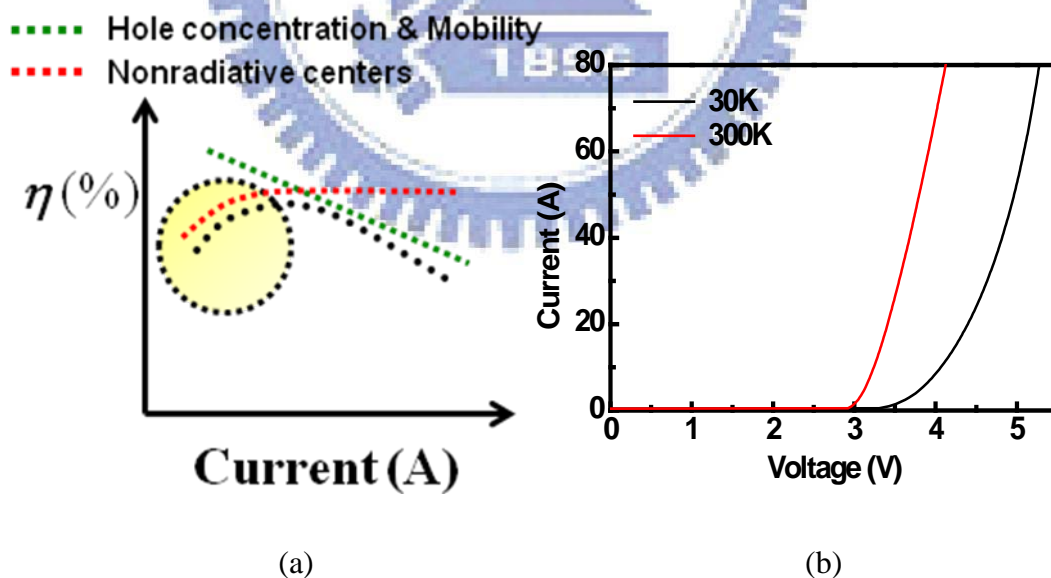
Fig. 5.3.2 (a) Schematic drawing of current dependence EL efficiency

(b) Current dependence forward voltage at 30K
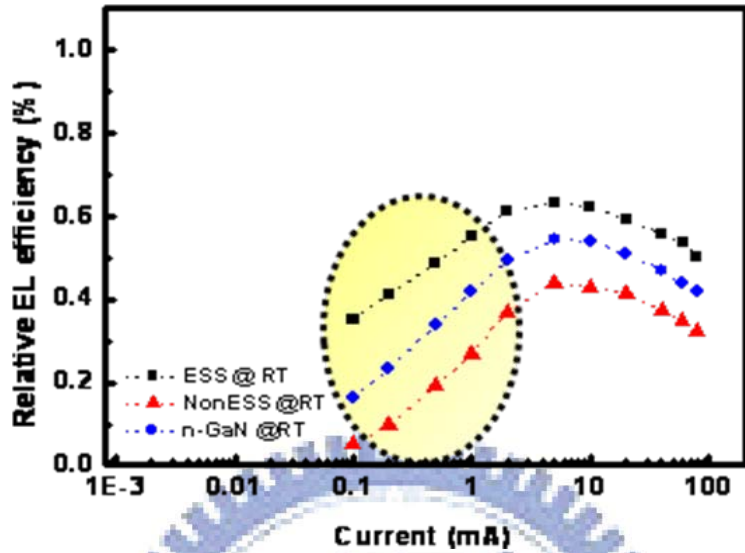
Fig. 5.3.3 Current dependence of the EL efficiency at 300 K

(a)   (b)
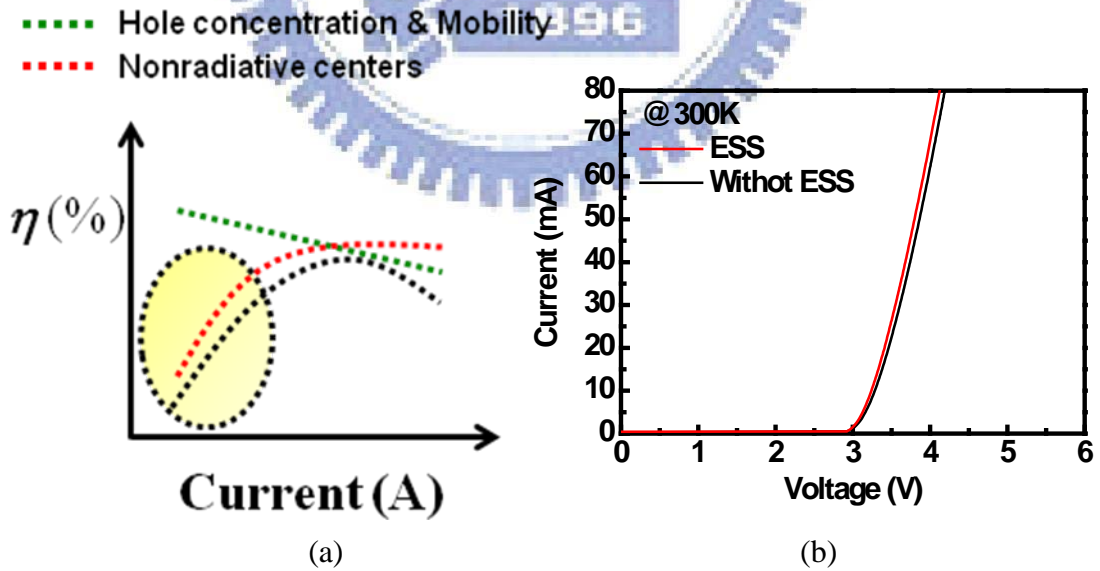
Fig. 5.3.4 (a) Schematic drawing of current dependence EL efficiency

(b) Current dependence forward voltage at 300 K

(a)
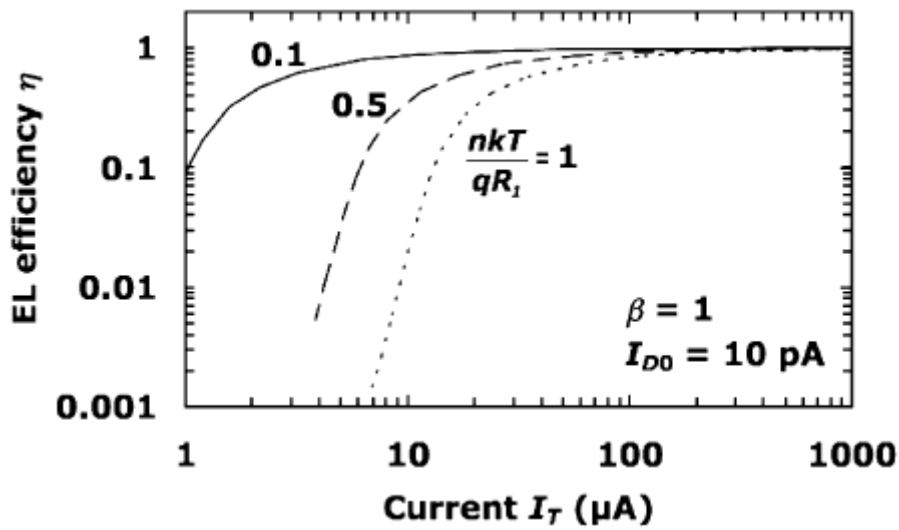
(b)

Fig. 5.4.1 (a) An equivalent circuit to represent the four current components: leakage
current I_{R1} by resistor R1, radiative current ID1 by diode D1,
nonradiative current ID2 by diode D2, and carrier-overflow current IR2
by resistor R2 with a switch.

(b) EL efficiency as a function of current in the low-current range,
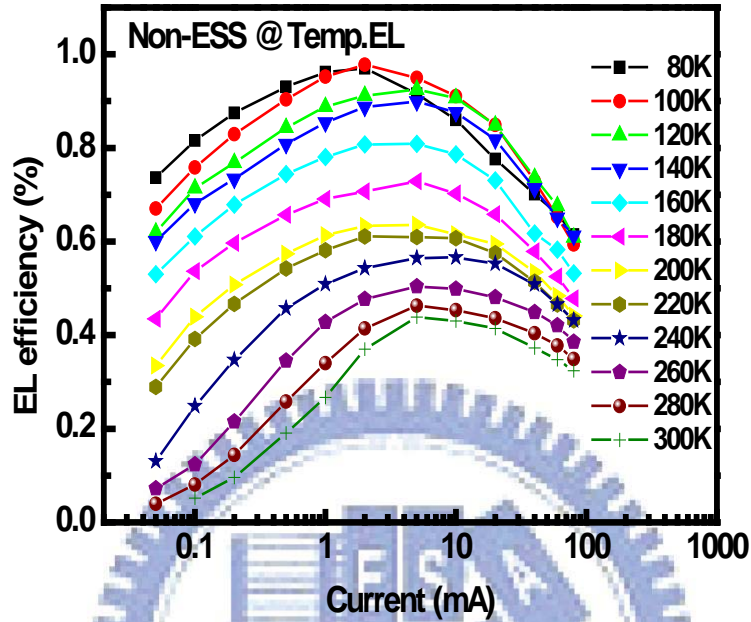
Fig. 5.4.2 Temperature dependent EL efficiency as a function of injection current of
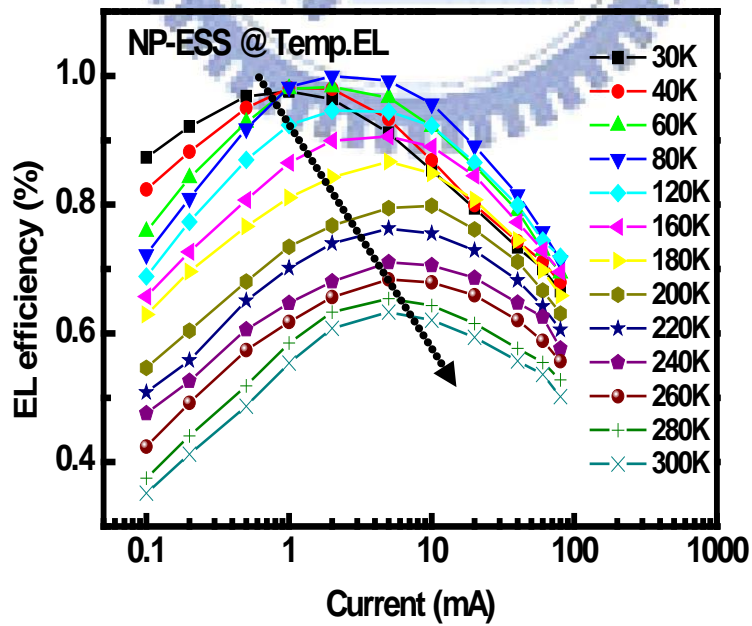without PSS InGaN/GaN UV LED

Fig. 5.4.3   Temperature dependent EL efficiency as a function of injection current of
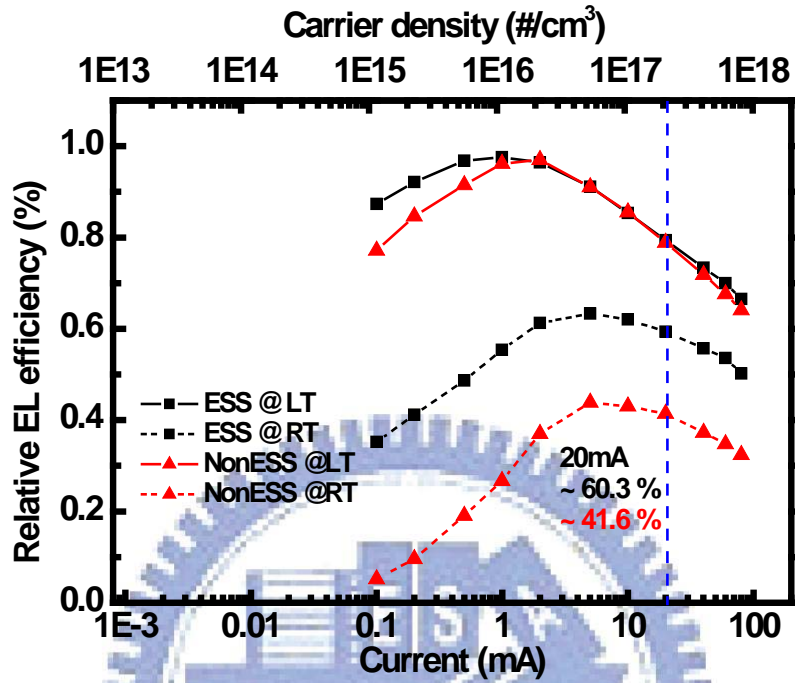PSS InGaN/GaN UV LED

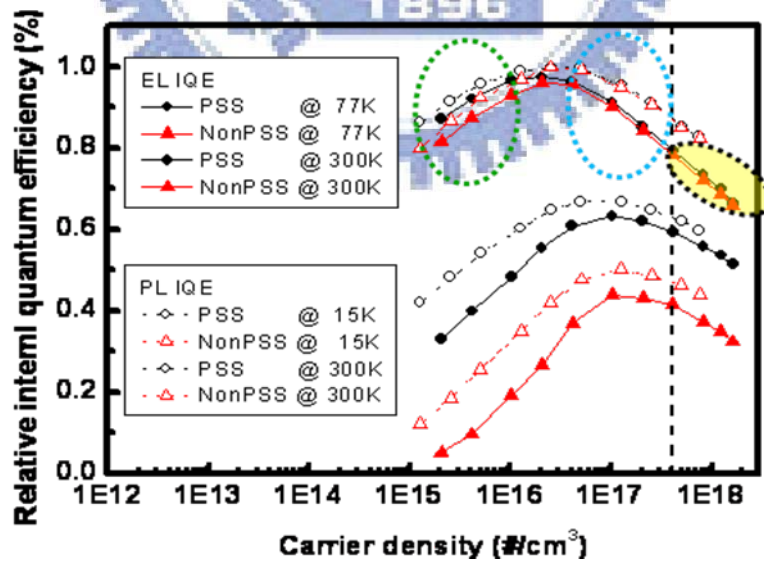Fig. 5.4.4 EL efficiency as a function of injection current at 77K and 300 K

Fig. 5.5.1 EL and PL efficiency as a function of injection current at low temperature

and room temperature

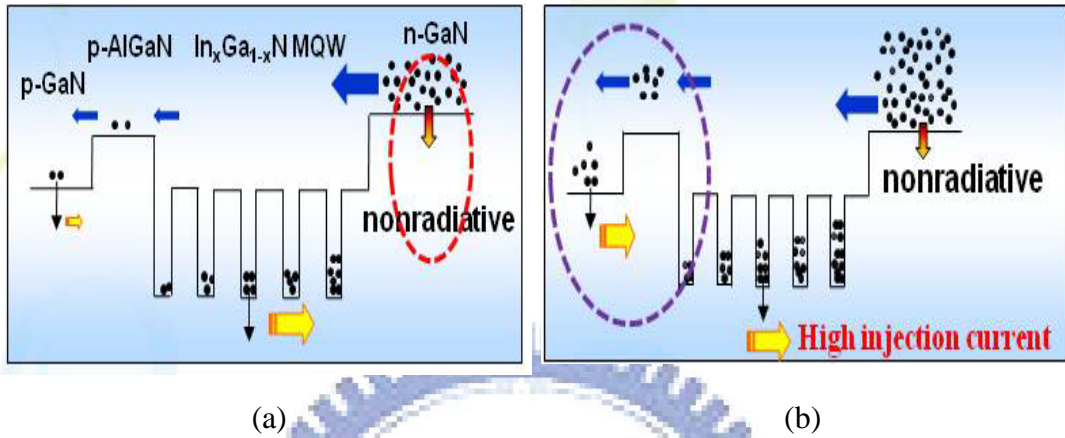(a)   (b)

Fig. 5.5.2 Schematic drawing of carrier transport at low and high injection current
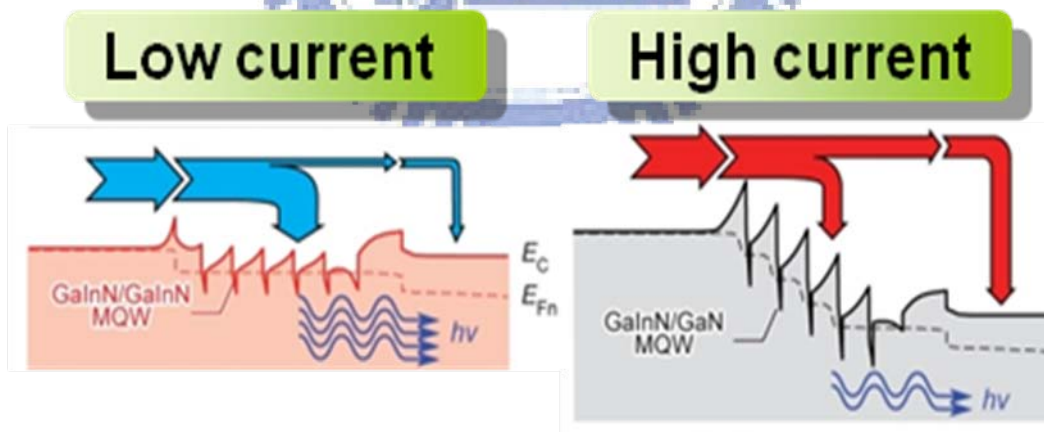

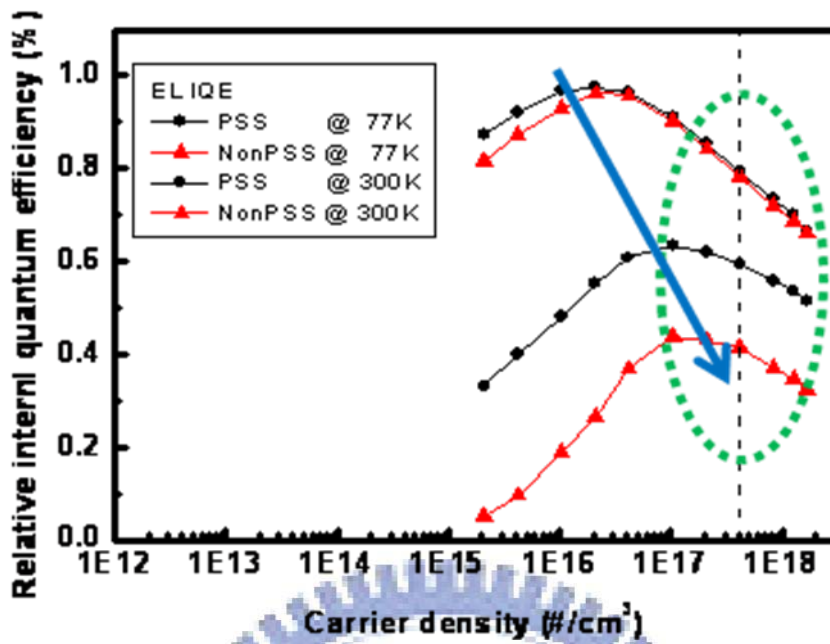Fig. 5.5.3 Efficiency droop mechanisms at low and high injection current

Fig. 5.5.4 EL Efficiency as a function of injection current of PSS and without PSS InGaN/GaN UV LED
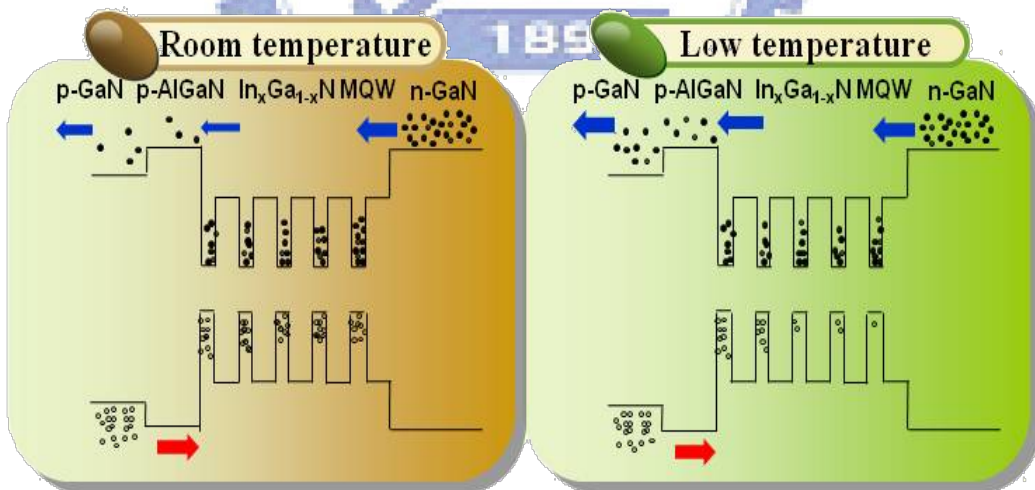

Fig. 5.5.5 Schematic drawing of electron and hole concentration distribution at low and high injection current
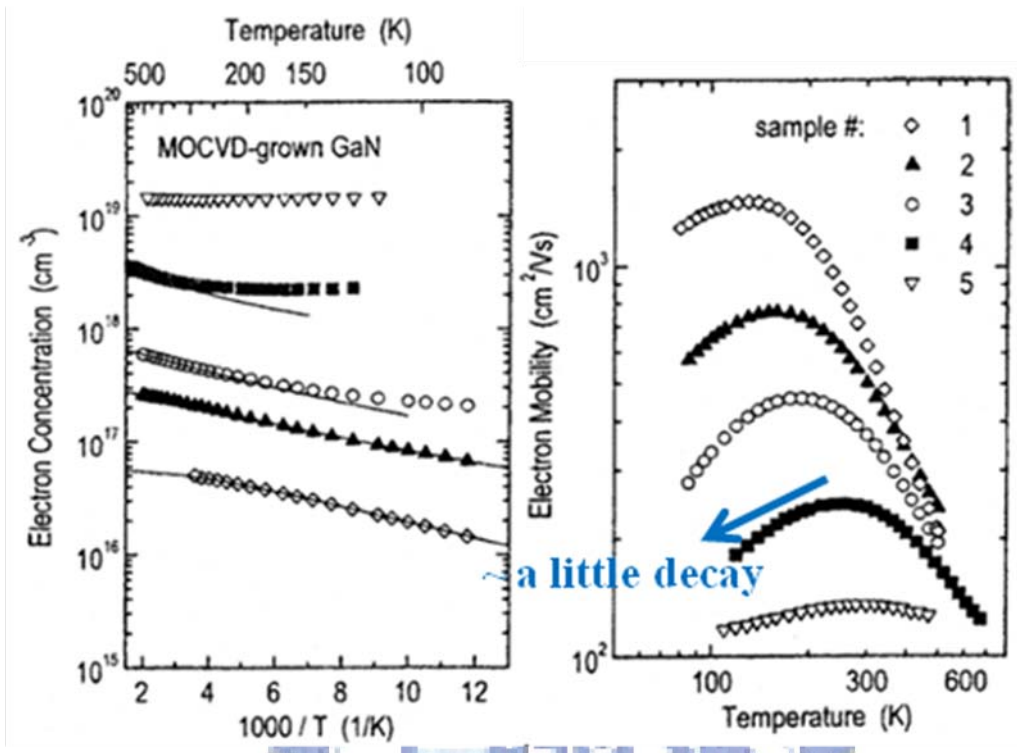
Fig. 5.5.6 Temperature dependence electron concentration and mobility

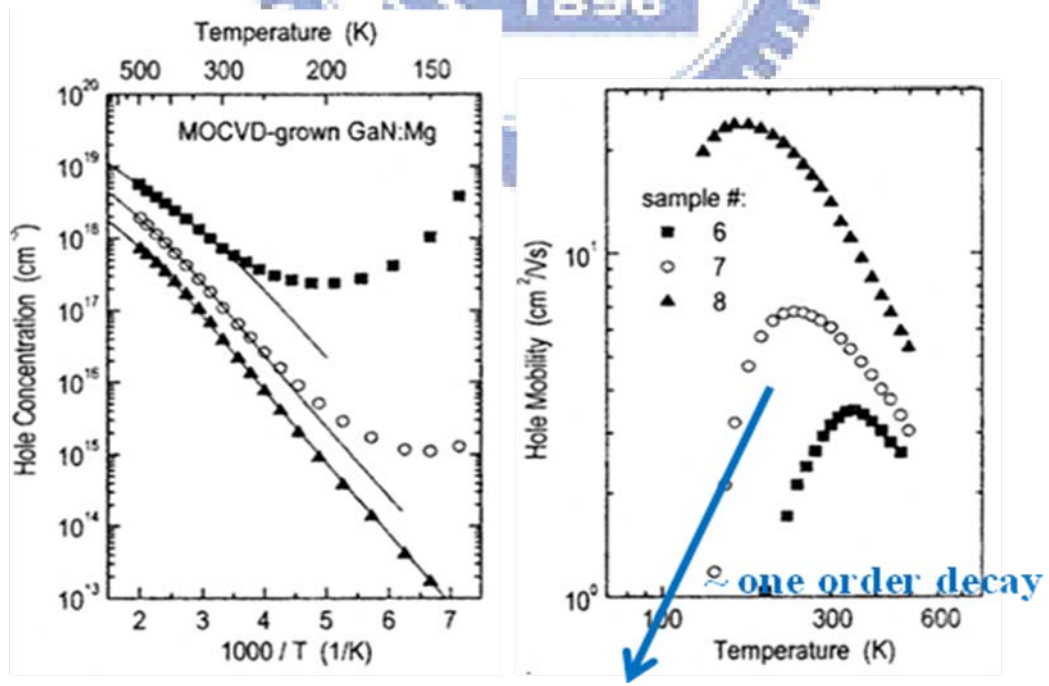Fig. 5.5.7 Temperature dependence hole concentration and mobility
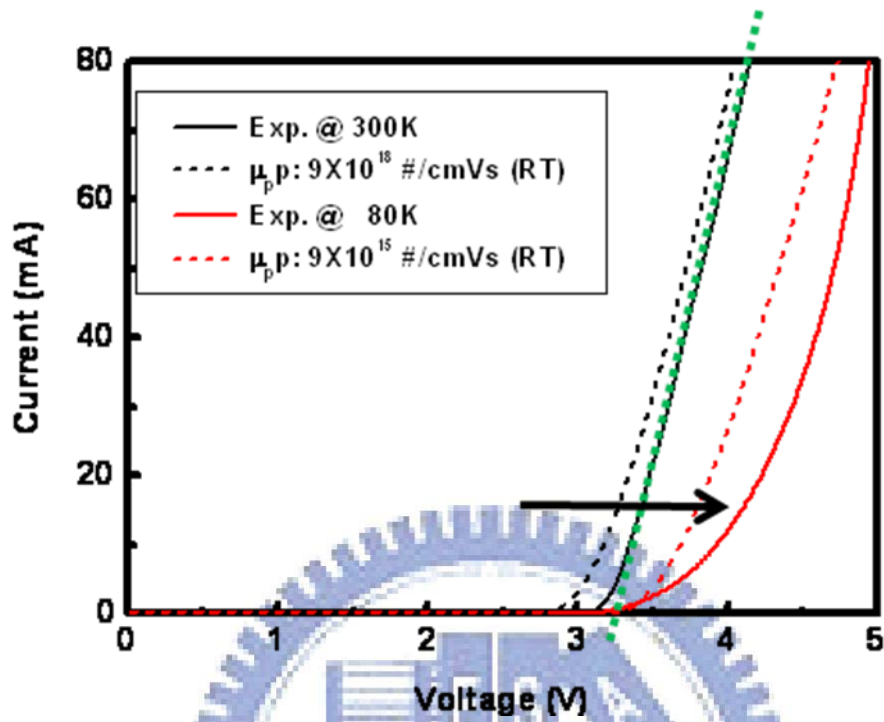
Fig. 5.6.1 I-V curve of simulation with different hole concentration and mobility

(a)   (b)
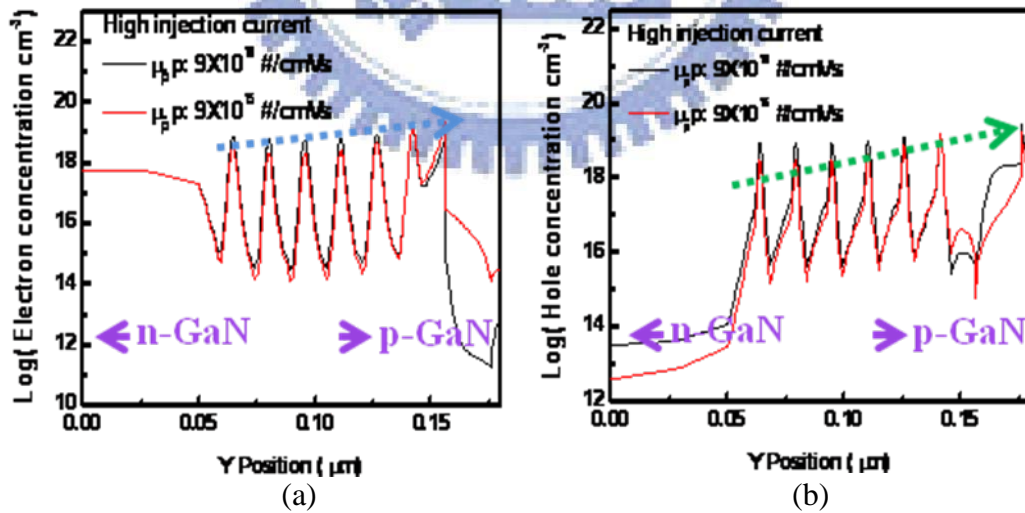
Fig. 5.6.2 Electron and hole concentration distribution at high injection current
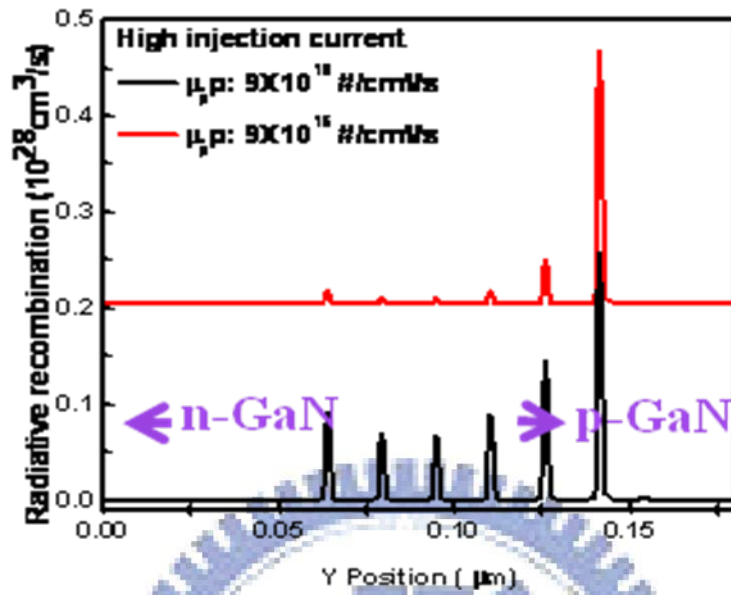
Fig. 5.6.3 Radiative recombination at high injection curret of InGaN/GaN MQW
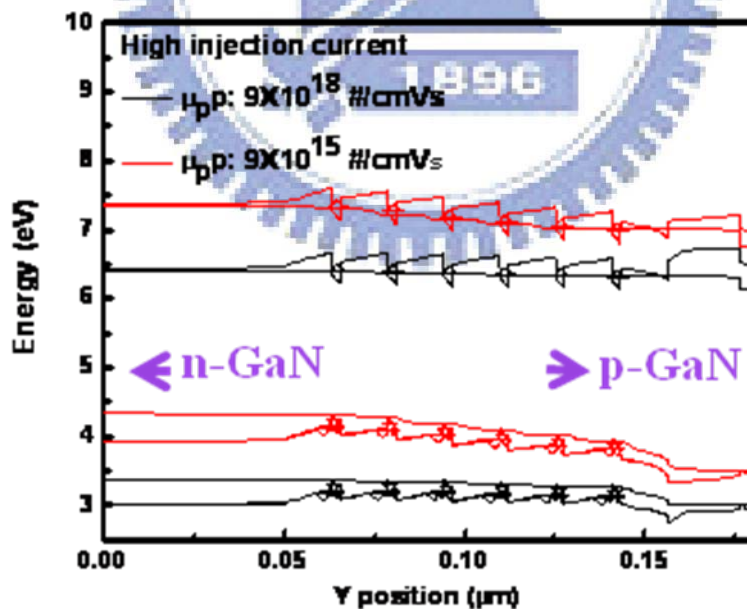
Fig. 5.6.4 Band diagram at high injection current of InGaN/GaN MQW

Table 5.4.2 Experimental PL IQE, EL IQE, and extraction efficiency

Sample	PL IQE(%)	EL IQE (%)	Exp. EQE (%)	PL Extraction (%)
PSS	~61.0%	~60.3%	43.0 %	~70.5%
Non-PSS	~44.2%	~41.6%	28.0 %	~63.3%

Chapter 6 Conclusion

From our analysis, we demonstrated the physical mechanisms which affect temperature dependence the PL efficiency and EL efficiency as a function of injected carrie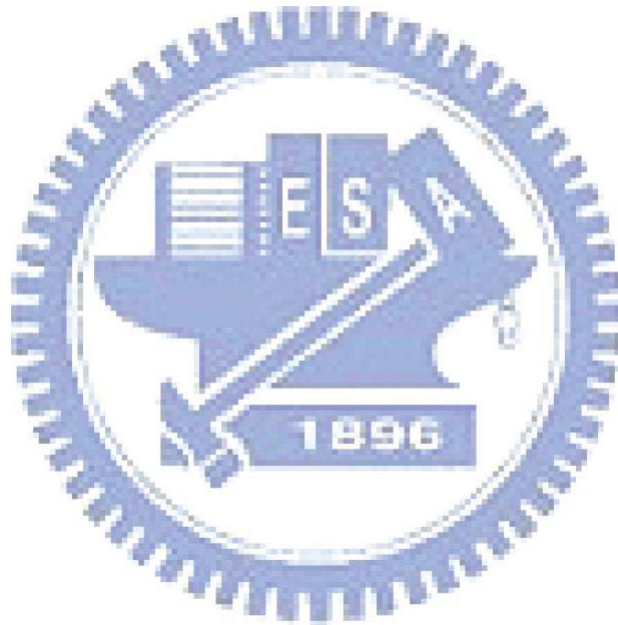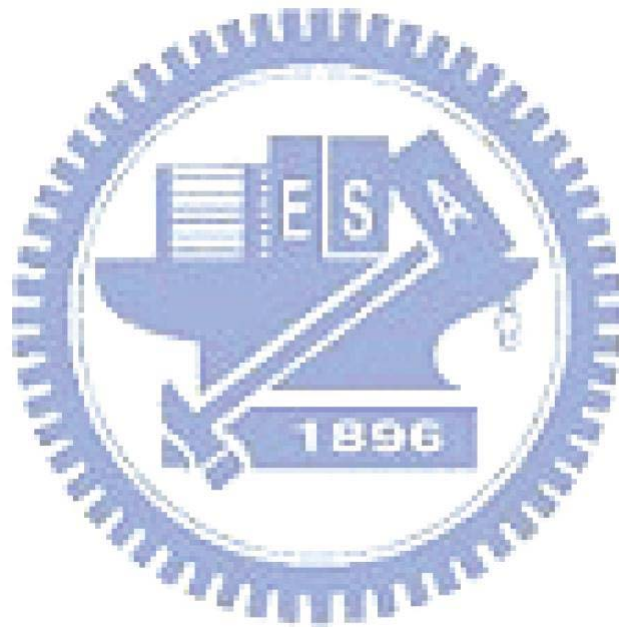r density. At low and room temperature, the nonradiative recombination centers and the carrier overflow mechanisms both play an important role in variation of quantum efficiency. In order to the deduction of compensate the nonradiative recombination centers to improve quantum efficiency at low injected carrier density, the improvement of crystal quality and reduced defects are necessary. But if the injected carriers keep increasing, the band filling effect and higher forward voltage will make carriers more easily escape from quantum well to p-GaN, resulting in deteriorating of quantum efficiency. Our results show the improvement of PL efficiency and EL efficiency by using PSS structure. We discussed the detail of temperature dependence PL and EL efficiency as a function of injected carrier density. We also used the theoretic method to calculate the IQE, the results coincide with our experimental IQE. And by the simulation of APSYS, we demonstrate the thermal generation of holes is insufficient and injected electrons continuously deplete holes, some of the injected electrons reach the p-GaN and exit the system without being able to recombine at low temperature. The phenomenon verified the EL efficiency droop more rapidly under this condition. To optimum the IQE and reduce the efficiency

droop, there many problem need to take care and improve. For example, decrease the

defect density, weakens the internal electric field in the QW, and increase the carrier

quantum confinement to make carrier hard escape from QW.

Reference

[1]   S. Nakamura, T. Mukai, and M. Senoh, Appl. Phys. Lett., 67, 1687 (1994)

[2]   S. Nakamura, M. Senoh, N. Iwasa, and S. Nagahama, Jpn. J. Appl. Phys., 34, L797 (1995)

[3]   G. Y. Xu, A. Salvador, W. Kim, Z. Fan, C. Lu, H. Tang, H. Markoc, G. Smith, M. Estes, B. Goldberg, W. Yank, and S. Krishnankutty, Appl. Phys. Lett., 71, 2154 (1997)

[4]   T. G. Zhu, D. J. H. Lambert, B. S. Shelton, M. N. Wong, U. Chowdhury, H. K. Kwon, and R. D. Dupuis, Electron Lett., 36, 1971 (2000)

[5]   G. T. Dang, A. P. Zhang, F. Ren, X. A. Cao, S. J. Pearton, H. Cho, J. Han, J. I. Chyi, C. M. Lee, C. C. Chuo, S. N. G. Chu, and R. G. Wilson, IEEE Trans. Electron Devices, 47, 692 (2000)

[6]   B. S. Shelton, D. J. H. Lambert, H. J. Jang, M. M. Wong, U. Chowdhury, Z. T. Gang, H. K. Kwon, Z. Liliental-Weber, M. Benarama, M. Feng, and R. D. Dupuis, IEEE Trans. Electron Devices, 48, 490 (2001)

[7]   A. P. Zhang, J. Han, F. Ren, K. E. Waldrio, C. R. Abernathy, B. Luo, G. Dang, J. W. Johnson, K. P. Lee, and S. J. Pearton, Electronchem. Solid-State Lett., 4, G39 (2001)

[8]   T. Matsuoka, H. Okamoto, M. Nakao, H. Harima, and E. Kurimoto, Appl. Phys. Lett., 81, 1246 (2002)

[9]   H. Morkoc, Nitride Semiconductors and devices, (Springer-Verlag, Berlin, 1999)

[10]   J. I. Pankove, E. A. Miller, and J. E. Berkeyheiser, J. Luminescence, 5, 84 (1992)

[11]   H. Amano, N. Sawaki, I. Akasaki, and Y. Toyoda, Appl. Phys. Lett., 48, 353 (1986)

[12]   H. Amano, N. Sawaki, I. Akasaki, and Y. Toyoda, Jpn. J. Appl. Phys., 28, L2112 (1989)

[13]   S. Nakamura, T. Mukai, M. Senoh, and N. Jwasa, Jpn. J. Appl. Phys., 31, 1258 (1992)

[14]   S. Chichibu, T. Azuhata, T. Sota, and S. Nakamura, Appl. Phys. Let., 69, 4188 (1996)

[15]   E. S. Jeon, V. Kozlov, Y.-K. Song, A. Vertikov, M. Kuball, A. V. Nurmikko, H. Liu, C. Chen, R. S. Kern, C. P. Kuo, and M. G. Craford, Appl. Phys. Lett., 69, 4194 (1996)

[16]   P. Perlin, V. Iota, B. A. Weinstein, P. Wisniewski, T. Suski, P. G.. Eliseev, and M. Osinski, Appl. Phys. Lett., 70, 2993 (1997)

[17] Y. Narukawa, Y. Kawakami, M. Funato, Sz. Fujita, S. Fujita, and S. Nakamura, Appl. Phys. Lett., 70, 981 (1997)

[18] I. H. Ho, Appl. Phys. Lett., 69, 2701 (1996)

[19] T. Mukai and S. Nakamura, Jpn. J. Appl. Phys., 38, 5735 (1999)

[20] M. Shatalov, A. Chitinis, V. Adivarahan, A. Lunev, J. Zhang, J. W. Yang, Q. Fareed, G. Simin, A. Zakheim, and M. Asif Khan, Appl. Phys. Lett., 78, 817 (2001)

[21] K. Tadatomo, H. Okagawa, Y. Ohuchi, T. Tsunekawa, Y. Imada, M. Kato, and T. Taguchi, Jpn. J. Appl. Phys., 40, L583 (2001)

[22] F. Bernardini and V. Fiorentini, Phys. Status Solidi B, 216, 391 (1999)

[23] A. Hangleiter, J. S. Im, H. Kollmer, S. Heppel, J. Off, and F. Scholz, MRS Internet J. Nitride Semicond. Res., 3, 15 (1998)

[24] K. Tadatomo, H. Okagawa, Y. Ohuchi, T. Tsunekawa, Y. Imada, M. Kato, and T. Taguchi, Jpn. J. Appl. Phys., 40, L583 (2001)

[25] J. J. Wierer, D. A. Steigerwald, M. R. Krames, J. J. O'Shea, M. J. Ludowise, G. Christenson, Y.-C. Shen, C. Lowery, P. S.Martin, S. Subramanya, W. Götz, N. F. Gardner, R. S.Kern, and S. A. Stockman, Appl. Phys. Lett., 78, 3379 (2001)

[26] D.-S. Han, J.-Y. Kim, S.-I. Na, S.-H. Kim, K.-D. Lee, B. Kim, and S.-J. Park, IEEE Photon. Technol. Lett., 18, 1406 (2006)

[27] H.-W. Huang, C. C. Kao, J. T. Chu, H. C. Kuo, S. C. Wang, and C. C. Yu, IEEE Photon. Technol. Lett.,17, 983 (2005)

[28] T. S. Kim, S.-M. Kim, Y. H. Jang, and G. Y. Jung, Appl. Phys. Lett., 91, 171114 (2007)

[29] M. Yamada, T. Mitani, Y. Narukawa, S. Shioji, I. Niki, S. Sonobe, K. Deguchi, M. Sano, and T. Mukai, Jpn. J. Appl. Phys., 41, L1431 (2002)

[30] T. S. Ko, T. C. Wang, R. C. Gao, Y. J. Lee, T. C. Lu, H. C. Kuo, S. C. Wang, and H. G. Chen, Appl. Phys. Lett., 90, 013110 (2007)

[31] D. L. Hibbard, S. P. Jung, C. Wang, D. Ullery, Y. S. Zhao, H. P. Lee, . So, and H. Liu, Appl. Phys. Lett., 83, 311 (2003)

[32] W.-K. Hong, J.O. Song, H.-G. Hong, K.Y. Ban, T. Lee, J. S. Kwak, Y. Park, and T.-Y. Seong, Electrochem. Solid-State Lett., 8, G320 (2005)

[33] I. V. Rozhansky and D. A. Zakheim, Phys. Status Solidi C 3, 2160 (2006)

[34] I. V. Rozhansky and D. A. Zakheim, Phys. Status Solidi A 204, 227 (2007)

[35] M. H. Kim, M. F. Schubert, Q. Dai, J. K. Kim, E. F. Schubert, J. Piprek, and Y. Park, Appl. Phys. Lett. 91, 183507 (2007)

[36] Y. C. Shen, G. O. Mueller, S. Watanabe, N. F. Gardner, A. Munkholm, and M. R. Krames, Appl. Phys. Lett. 91, 141101 (2007)

[37] A. A. Efremov, N. I. Bochkareva, R. I. Gorbunov, D. A. Larinovich, Yu. T.

Rebane, D. V. Tarkhin, and Yu. G. Shreter, Semiconductors 40, 605 (2006)

[38] A. Y. Kim, W. Götz, D. A. Steigerwald, J. J. Wierer, N. F. Gardner, J. Sun, S. A. Stockman, P. S. Martin, M. R. Krames, R. S. Kern, and F. M. Steranka, Phys. Status Solidi A 188, 15 _2001_.

[39] S. F. Chichibu, T. Azuhata, M. Sugiyama, T. Kitamura, Y. Ishida, H. Okumurac, H. Nakanishi, T. Sota, and T. Mukai, J. Vac. Sci. Technol. B 19, 2177 (2001)

[40] C. Kisielowski, J. Kru¨ger, S. Ruvimov, T. Suski, J. W. Ager III, E. Jones, Z. Liliental-Weber, M. Rubin, and E. R. Weber, Phys. Rev. B, 54 17745 (1996)

[41] GaN and Related Materials, S. J. Pearton

[42] J. H. Lee, J. T. Oh, J. S. Park, J. W. Kim, Y. C. Kim, J. W. Lee, and H. K. Cho, Phys. Stat. Sol. (c), 3, 2169 (2006)

[43] J. Wang , L.W. Guo, H.Q. Jia, Z.G. Xing, Y. Wang, H. Chen, J.M. Zhou, Thin Solid Films 515, 1727 (2006)

[44] S. Watanabe, N. Yamada, Appl. Phys. Lett. 83, 4906 (2003)

[45] I. Ho and G. B. Stringfellow, Appl. Phys. Lett. 69, 2701 (1996)

[46] Q. Dai, M. F. Schubert, M. H. Kim, J. K. Kim, E. F. Schubert, D. D. Koleske, M. H. Crawford, S. R. Lee, A. J. Fischer, G. Thaler, and M. A. Banas Appl. Phys. Lett., 94, 111109 (2009)

[47] A. Hori, D. Yasunaga, A. Satake, and K. Fujiwara, Appl. Phys. Lett. 79, 3723 (2001)

[48] C. M. Lee, C. C. Chuo, J. F. Dai, X. F. Zheng, and J. I. Chyi, J. Appl. Phys. 89, 6554 (2001)

[49] C. L. Yang, L. Ding, J. N. Wang, K. K. Fung, W. K. Ge, H. Liang, L. S. Yu, Y. D. Qi, D. L. Wang, Z. D. Lu, and K. M. Lau, J. Appl. Phys. 98, 023703 (2005)

[50] S. Grzanka, G. Franssen, G. Targowski, K. Krowicki, T. Suski, R. Czemecki, P. Perlin, and M. Leszczyski, Appl. Phys. Lett. 90, 103507 (2007)

[51] P. Bakmiwewa, A. Hori, A. Satake, K. Fujiwara, Physica E 21, 636 (2004)

[52] H. Masui, T. Ive, M. C. Schmidt, H. Sato, H. Asamizu, S. nakamura, and S. P. Denbaars, Jpn. J. Appl. Phys., 47, 2112 (2008)

[53] D. Steigerwald, S. Rudaz, H. Liu, R. S. Kern, W. Gotz, and R. Fletcher, JOM, volume 49, 18 (1997)